CRANFIELD UNIVERSITY

JIAN ZHANG

Molecular Dynamics Study of Effects of Vacancy on Phonon Heat Conductivity of Copper

School of Aerospace, Transport and Manufacturing

MSc Thesis

MSc by Research

Academic Year: 2014 - 2015

Supervisor: Dr. Karl Jenkins

September 2015

CRANFIELD UNIVERSITY

School of Aerospace, Transport and Manufacturing

MSc

Academic Year 2014 - 2015

JIAN ZHANG

Molecular Dynamics Study of Effects of Vacancy on Phonon Heat Conductivity of Copper

Supervisor: Dr. Karl Jenkins
September 2015

ABSTRACT

Heat conductivity is an important property for solids, which exhibits their ability of transporting heat. It is composed of two parts, heat conductivity contributed by electrons and that by phonons. By experiments, heat conductivity of many materials has been calculated. For instance, Copper (Cu) has a good heat conductivity of about 400 W/mK, while the heat conductivity of glass (0.78 W/mK) is much less than it. Due to the high heat conductivity of Cu, it has been found in various applications, such as heat sinks and heat pipes. Although a great many researchers have investigated the heat conductivity of Cu in experiments, one can not understand the heat transfer mechanism in a view of microscopic.

Molecular dynamics (MD) originated as a simulation method in the late 1950s. Due to the increasing advances in computer technology and algorithmic promotion, MD has become a precious tool in many fields of physics and chemistry. The phonon heat conductivity of perfect Cu has been investigated using MD. However, in reality, it is practically impossible to manufacture a piece of Cu without defects. Generally, there are a variety of defects, such as vacancy, dislocations and grain boundary, existing in materials. Note that vacancy is the simplest defect in materials.

The objective of this research is to make a MD model and study the relationship between vacancy and phonon heat conductivity of Cu. Models are implemented mainly in four temperatures, 50 K, 300 K, 1000 K and 1300 K. The main finding is that the phonon heat conductivity decreases with the increasing vacancies. Following this realization, an analysis of the system is carried out to understand the mechanism of phonon heat transfer.

Keywords:

Phonon heat conductivity, Vacancy, Molecular Dynamics, Green-Kubo Method, copper

ACKNOWLEDGEMENTS

First of all, I would like to express my gratitude to my supervisor, Dr. Karl W Jenkins for his constant help, support and guidance.

I would also like to sincerely thank Dr. Michalis Frank for his support and advice in the whole study. He taught me how to manage the research study and use some MD software (such as, VMD and LAMMPS). Without his help, the thesis could not been completed successfully.

I am also very grateful to Commercial Aircraft Corporation of China for supplying this excellent opportunity of studying at Cranfield University.

I would also like to give a special appreciation to all my colleagues and friends in Cranfield University, because who made my life in Cranfield significantly wonderful.

Finally, most of my gratitude goes to my family, my parents, wife and daughter, for their continuous support, concern and encouragement throughout the past years.

TABLE OF CONTENTS

LIST OF FIGURES

LIST OF TABLES

LIST OF ABBREVIATIONS

BCC	Body-centered Cubic
CPU	Central Processing Unit
EAM	Embedded Atom Method
EMD	Equilibrium Molecular Dynamics
FCC	Face-centered Cubic
GNR	Graphene Nanoribbon
GPU	Graphics Processing Unit
HCACF	Heat Current Autocorrelation Function
HCP	Hexagonal Close-packed
HPC	High Performance Computer
LAMMPS	Large-scale Atomic/Molecular Massively Parallel Simulator
LJ	Lennard-Jones
MC	Monte Carlo
MD	Molecular Dynamics
MEAM	Modified Embedded Atom Method
MEMS	Microelectromechanical Systems
NEMD	Non-equilibrium Molecular Dynamics
NPT	Isothermal-isobaric Ensemble
NVE	Microcanonical Ensemble
NVT	Canonical Ensemble
PBC	Periodic Boundary Condition
VMD	Visual Molecular Dynamics

1 Introduction

1.1 Application of Heat Transfer

Copper (Cu) is one of most common metals in nature. Its atomic number is 29 and it belongs to the group 11 of the chemistry element periodic table. Copper is widely used in many fields due to its high electrical and heat conductivity.

In the aspect of heat transfer, copper has become the main material in various heat devices, such as, heat pipes and heat sinks.

Heat pipe is a common heat dissipate device in computer, and its key function is to maintain the electronic components, such as Central Processing Unit (CPU) and Graphics Processing Unit (GPU), at a safe operating temperature. (Figure 1-1)

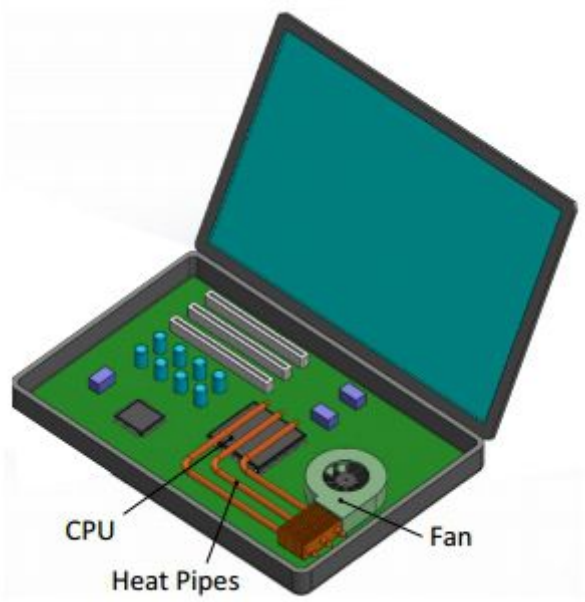

Figure 1-1 A schematic of a laptop cooling system, which is mainly composed of heat pipes and fan. [1]

With the development of manufacturing techniques, nano-scale electronic components have been produced. However, in the meantime, it gives rise to abundant heat needing to be dissipated. Hence, this circumstance places a greater demand on thermal property study of materials of heat pipes.

1.2 Heat Transfer

Heat transfer is the phenomenon of the rules governing the transfer of heat between systems of different temperatures. Figure 1-2 shows a simple example of heat transfer application. A radiator, in which hot water flows, is installed in a room to obtain a fix room temperature. The designer should take account of various parameters, such as the room temperature, the required heat flow rate, heating water temperature and mass flow rate, to make the radiator not only cheap but also efficient. The exact above knowledge required is just what heat transfer studies.

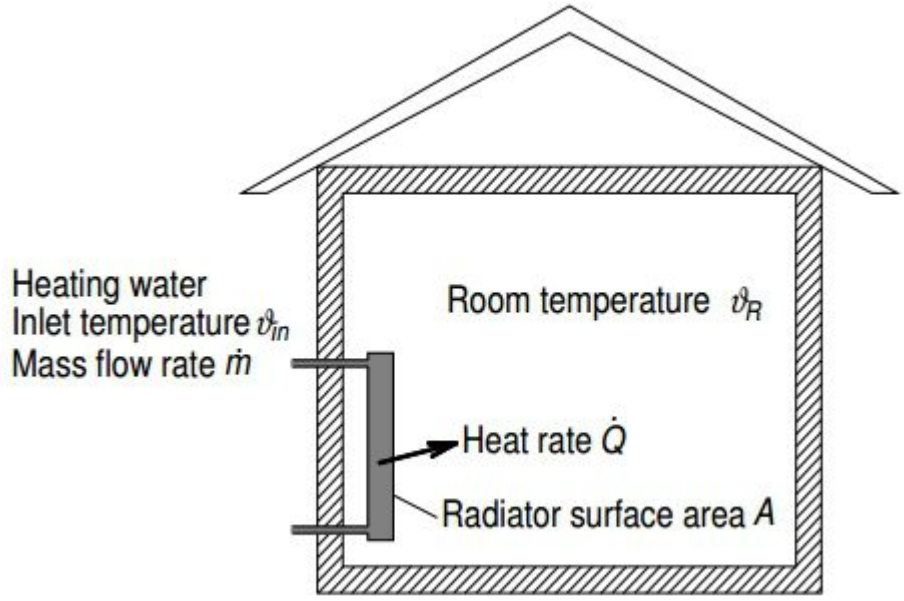

Figure 1-2 A schematic of a radiator design. [2]

It is well-known that there are three modes of heat transfer: heat conduction, heat convection and heat radiation. Heat conduction is the transfer of energy between systems in contact in the presence of a temperature gradient. Heat conductivity is an important concept to describe the ability of transporting heat in materials.

In general, heat conductivity consists of two parts, heat conductivity contributed by electrons and that by **phonons** (lattice vibrations which carry energy), in general. For non-metals or **dielectric materials** (which is a substance that is a

poor conductor of electricity, such as, ceramic, glass, and mica), the heat transfer of vibration (by phonons) is the main mode, while the contribution from electrons is neglected at all times. Contrary to non-metals and dielectric materials, heat in metals is mostly transferred through electrons.

1.3 Modelling of heat transfer

Molecular Dynamics (MD), which originated in the late 1950s, is an excellent tool to study complex systems in an atomic level by means of computer codes. Figure 1-3 shows the study range of time and length scales in molecular dynamics. Beyond the range, other computational methods should be needed. Currently, the method has been popular in chemical biology, chemistry and physics. It assists in the link between macroscopic computational model and experimental results. Moreover, molecular dynamics simulation provides microscopic information, such as the position and momentum of every atom, unavailable in experiments, which can be used to understand the macroscopic behaviour of the system.

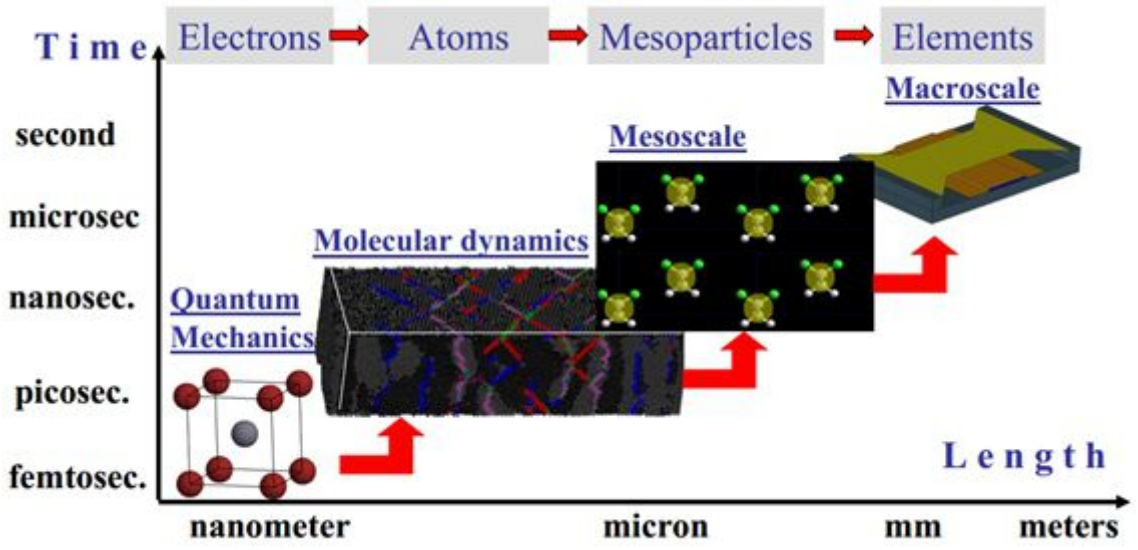

Figure 1-3 A schematic of how to select an appropriate computational method taking consideration into a specific size and time. [3]

Great achievements have been made in the field of heat transfer using MD method. Two common computational models of heat transfer are the direct

method and the Green-Kubo method. The direct method is a non-equilibrium molecular dynamics (NEMD) method, while the other one is an equilibrium molecular dynamics (EMD) method. [4] Although both of them have been proven to be available in calculating the heat conductivity in many materials, they are incompetent to compute the total heat conductivity of metals correctly due to the lack of contribution from electrons. Consequently, few researchers have studied the heat conductivity of metals in molecular dynamics.

In this thesis, we use the Green-Kubo method.

1.4 Motivation

With rapid development of materials science, the size of electronic components is becoming less and less. The heat conductivity is of much importance for these devices because electronic components with a small size scale are easier to overheat. Many researchers have begun to study phonon heat conductivity in metals (for example, the influence of phonon in low-dimensional system is worse than that in the bulk metals). The study of phonon heat conductivity of metals may supply valuable information for choosing proper materials in electronic components. However, until now, there are very few achievements in the fundamental field of phonon heat conductivity of metals using MD method. This thesis, as a fundamental research, focuses on how vacancy (the simplest defect) effects phonon heat conductivity of copper.

1.5 Modelling Tools

1.5.1 LAMMPS

LAMMPS (Large Scale Atomic/Molecular Massively Parallel Simulator) is an open-source code developed by Sandia National Lab [7], which is used to implement molecular dynamics simulation in this thesis. LAMMPS uses different techniques for the computation of interatomic interactions, potentials, neighbour list and cutoff distance. It has a great number of features, such as, its extensibility (since it is open source), good parallel performance, well-organized documents and active user community.

1.5.2 VMD

Visual molecular dynamics (VMD) is a molecular modelling and visualization computer program, which can be employed to animate and analyze the trajectory of a molecular dynamics simulation. [8] The main feature is that it can provide a graphic display of molecules, which is beneficial to understand molecules in a microscopic view.

1.5.3 ASTRAL

ASTRAL-2 High Performance Computer (HPC) is a large independent Linux cluster intended for advanced study needing a great deal of computation, which is composed of 80 compute nodes. Each node is consisted of two Intel E5-2660 (Sandy Bridge) CPUs giving 16 CPU cores, 72 nodes have 64 GB shared memory and the remaining 8 nodes have 128 GB of share memory. Totally ASTRAL-2 has 1280 available cores can be applied for computing. The theoretical peak processor performance (R_{peak}) is 22.5 TFlops and the measured maximum performance (R_{max}) is 18.8 TFlops. [9] The scripts of LAMMPS can be implemented in ASTRAL-2.

1.5.4 Origin

Origin, which is developed by OriginLab Corporation, is an advanced software for data analysis and scientific graphing. Top features include enhanced statistical repertoire, 3-D fitting, peak fits, axis dialog and image processing. [10] Moreover, the interface of Origin is much friendly for new beginners.

1.6 Aims and Objectives

The aim of this project is to better understand how vacancies effect the phonon heat transfer behaviour in metals.

The objectives of the project are as followed:

- To develop related molecular dynamics models of heat transfer about copper and validate them against results from the literature.

- To investigate the relationship between vacancy and phonon heat conductivity in pure Cu
- To analyse the behaviour of the system in an attempt to provide insight into the mechanism of phonon heat transfer

1.7 Thesis Overview

In Chapter 2, the literature review of the thesis is presented. The main goal of this chapter is to introduce the gap.

Chapter 3 describes some fundamental concepts of crystalline solids and heat transfer. Initially, an introduction is made to crystal structures and vacancy (point defect). Lastly, this chapter explains the mechanism of heat transfer, especially in solids.

Chapter 4 describes the details of the technique, method and process of molecular dynamic simulation in the beginning. Finally, the rest of this chapter is dedicated to two common models of calculating the heat conductivity in molecular dynamics.

Chapter 5 illustrates the basic MD model of this work used to gain the phonon heat conductivity. The remainder of this chapter presents the validation of the model.

Chapter 6 describes the effect of vacancy on phonon heat conductivity in copper. Models are studied in four temperatures, 50 K, 300 K, 1000 K and 1300 K. At last, analysis and discussions are presented.

Chapter 7 gives the conclusions of this work and recommendation for the future work.

2 Literature review

This chapter describes the whole process of choosing the research direction. Initially, an introduction to application of heat transfer in metals is presented. Then the review mentions the effect of defects and alloying element on heat conductivity. Finally, extensive researches of heat conductivity in molecular dynamics are proposed. Based on the previous researches, the research direction of this thesis is determined, which is to investigate the phonon heat conductivity of copper with vacancies in molecular dynamics method.

2.1 Application of heat transfer in metals

Owing to high heat transport efficiency, metals are widely applied in many industrial applications, for example, heat exchanger, heat sink and heat pipes.

Various kinds of metals, such as copper, aluminium and nickel, are often used in heat exchangers. As aluminium has a good balance between higher heat conductivity and less weight in a lower temperature, they are applied as core material in plate-fin heat exchangers (see Figure 2-1). [11]

Heat sinks are the most common and cost-effective hardware employed for the thermal management of microelectronic circuits and **microelectromechanical systems** (**MEMS**) devices. A **heat sink** is a device that absorbs and dissipates heat from another object using thermal contact [11]. Among all the factors affecting the performance of a heat sink, thermal conductivity of the materials used is the key point. Due to the high heat conductivity of metals, they are used widely in heat sinks. A heat sink usually consists of a base with one or more flat surfaces and an array of comb or fin-like protrusions to increase the heat sink's surface area contacting the air, and thus increasing the heat dissipation rate. (see Figure 2-2)

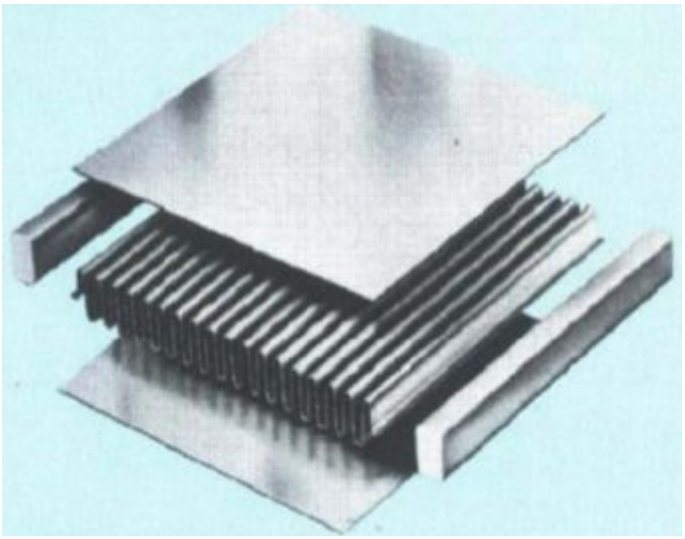

Figure 2- 1 Plate-fin heat exchanger[12]

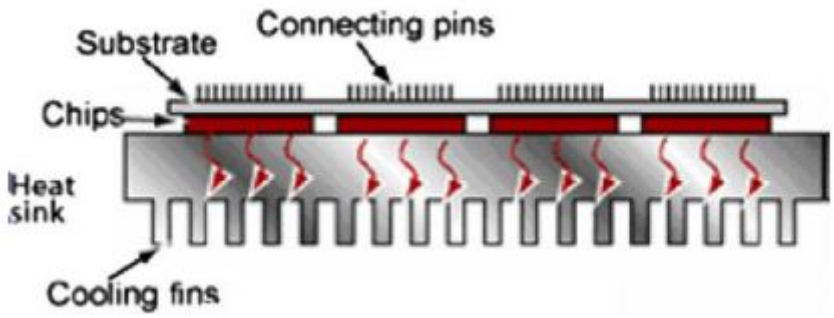

Figure 2- 2 Common design of a heat sink [11]

The **heat pipe**, is a heat spreader used for cooling the CPU in a notebook or a desktop PC. Heat pipes (see Figure 2-3) utilize evaporative cooling to transfer thermal energy from one point to another by the evaporation and condensation of a working fluid or coolant. The phase change of working fluid, like evaporation and condensation, needs much energy exchange, which enhances the heat transfer of heat pipes. The selection of working fluid and pipe wall material is an important work for heat pipes. Generally, copper, due to the high heat conductivity, is used in heat pipe wall. [13]

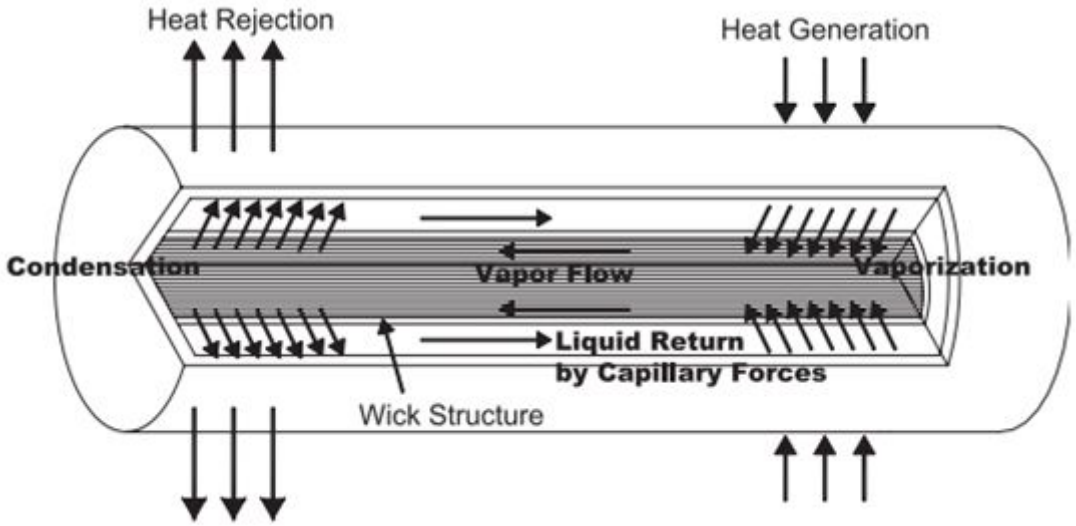

Figure 2-3 A schematic graph of heat pipes [13]

2.2 The Study of Heat Conductivity of Metals and alloys

This section describes two ways of effecting the thermal transport of metals. The first one is to introduce defects in metal, and the other one is to insert a new element into the metal base and make it become alloy. Heat conductivity is a vital physics term, which is used to describe the ability of transporting heat of materials. In this section, heat conductivity is the main part studied in the field of heat transfer.

2.2.1 Effect of defects on heat conductivity

In pure metals, electrons account for the major contribution of heat transfer, whereas phonon heat conductivity is commonly neglected. However, electrons may not play a vital role in alloys, such as PbTe alloy [14]. Defects effect the heat transport of metals. [15]

Powder metallurgy is the process in which materials are made from metal powders. The defects, such as porosity and voids, are inevitably introduced in manufacturing processes, which have adverse effects on the thermal property of materials. As indicated in Figure 2-4 , the heat conductivity of copper originating from dendritic copper powder decreases with volume fraction of porosity, and in domain II, it falls more sharply than the other two.[15] In general,

during the initial stage of the sintering process the porosities are interconnected (open) and become isolated (closed) as the densification proceeds. It is well seen that the transition from open to closed porosities occurs at around 6% of porosity. Since, domain III and domain I presents the initial open porosity and closed porosity, respectively, the transition occurs in domain II. Therefore, heat conductivity in domain II has a significant decrease compared with that in domain I and domain III.

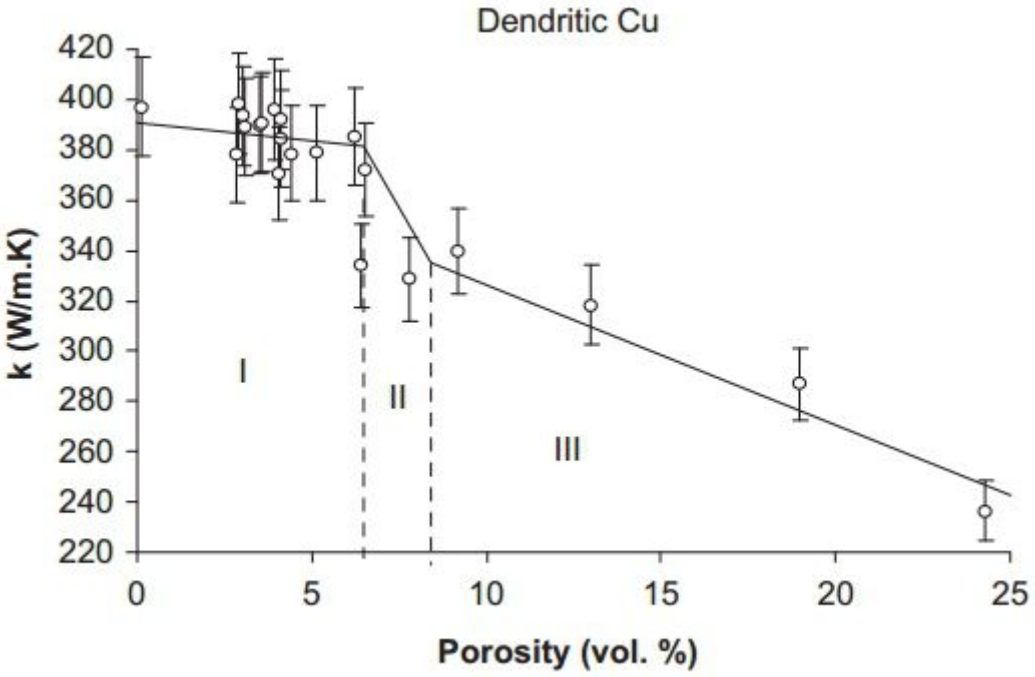

Figure 2-4 The heat conductivity of copper as a function of the volume fraction of porosity. [15]

In thermoelectric devices fields, the higher ZT values materials are paid more attention on. PbTe-based alloys are chosen as thermoelectric materials due to their low heat conductivity and high power factors (see Section 2.3.1). Inducing Sb **nanoparticles** (particles between 1 and 100 nanometers in size) in PbTe alloy succeeds in lowering lattice or phonon heat conductivity greatly, which attributes the main part of heat conductivity.[16] Besides introducing nanoscale particles, reducing grain sizes of PbTe alloy is also a good method to decrease phonon heat conductivity for improving the thermoelectric performance of materials.[14]

2.2.2 Effect of alloying on heat conductivity

Generally, the process of adding varied kinds of alloying elements in a metal base could result in totally different thermal properties. Aiming at understanding how alloying elements effect heat conductivity, it is essential to figure out the heat conductivity of binary alloys.

Magnesium alloys have been investigated in the condition of binary alloys, such as Mg-Al alloy [17] and Mg-Zn alloy [18]. Take Mg-Al alloy for example, there are three binary Mg-Al alloys are fabricated by casting, 0.5%, 0.9% and 1.5% are the composition in atomic percentage of Mg-0.5Al alloy, Mg-0.9Al alloy and Mg-1.5Al alloy respectively. The heat conductivity declined significantly by inducing Al element into pure Mg. In as-cast Mg-0.9Al and Mg-1.5Al alloy, the heat conductivity goes up with temperature, while there is an opposite trend in as-cast pure and Mg-0.5Al alloy.(see Figure 2-5)[17]

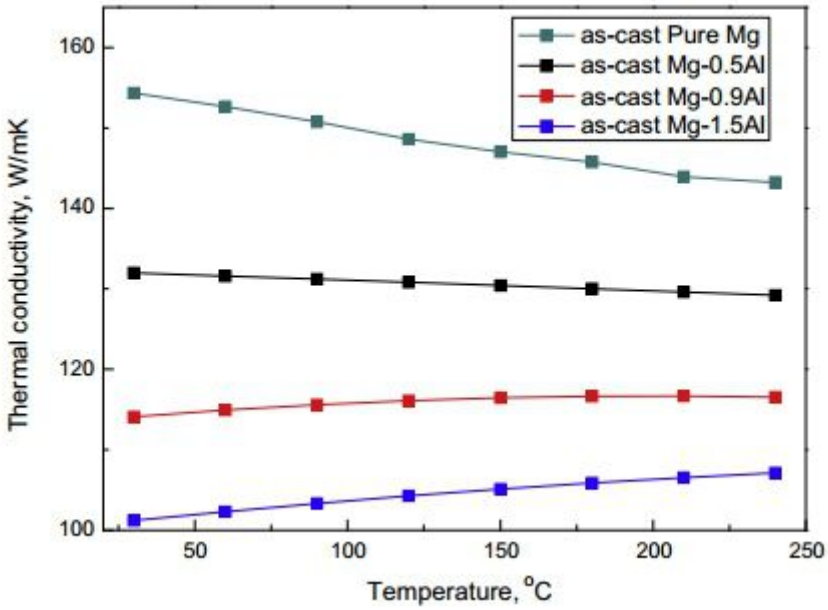

Figure 2- 5 Heat conductivity of as-cast Mg-Al alloys. [17]

Figure 2-6 illustrates the heat conductivity of as-cast Mg-Zn alloys. By comparison, Al shows a relatively stronger effect in heat conductivity than Zn. For instance, in case of 0.5% composition, heat conductivity of as-cast Mg-0.5Al alloy decreases much more than that of as-cast Mg-0.5Zn alloy.

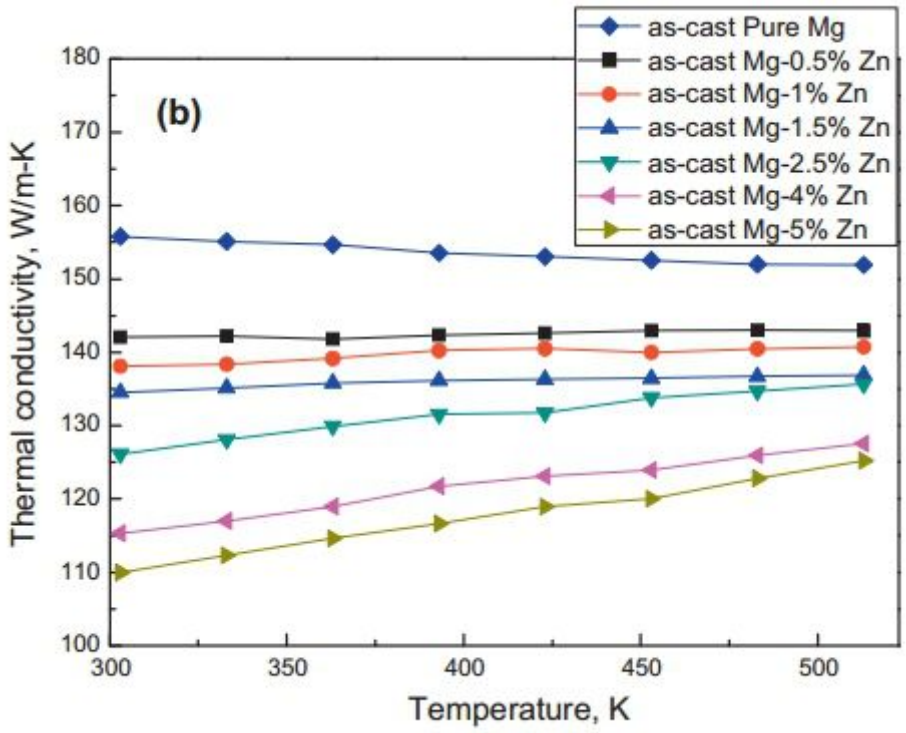

Figure 2- 6 Heat conductivity of as-cast Mg-Zn alloys. [18]

2.2.3 Summary

This section presents two styles of impacting the heat conductivity on metallic materials. There have been a great deal of studies about the thermal property of metals in experiments. However, to date, we can not understand the heat transfer of metals in a microscale perspective clearly. Because of that, the thesis changes the research direction to molecular dynamics study of heat property in metals.

2.3 Molecular Dynamics of Heat Transfer

Molecular dynamics (**MD**) has been proven an excellent tool in studying the heat conductivity. Nonetheless, the range of MD is only limited to phonon heat conductivity. As most non-metals and alloys transport the heat by phonons [19], there have been a great number of relevant papers republished using MD during the last few decades. Compared with non-metals and alloys, far fewer investigations on heat conductivity of metals in MD have been done.

2.3.1 Non-metals and alloys

Here we present some molecular dynamics research about heat conductivity in non-metals and alloys.

Argon, is an ideal material for the study of molecular dynamics to present phonon heat conductivity. First, the Lennard-Jones pair potential is known to describe the interatomic forces adequately for argon. Second, there are experimental data used to confirm the validity of the results of the molecular dynamics simulations.[20,21] In low temperature, **heat current autocorrelation function** (**HCACF**)(see Section 4.8.2) shows a distinct two-stage decay, which consists of an initial rapid decay associated by local dynamics and a slower decay associated with the lattice vibration dynamics.[5,22] On the condition that the error between simulation and experiments is estimated 5-10%, the values of heat conductivity of argon crystal by molecular dynamics have a good agreement with experiments in 10, 20, 30, 70 K, while there is a underestimate at 40 and 50 K.[5](Figure 2-7) The study about argon in molecular dynamics promotes the development of thermal transfer of other materials.

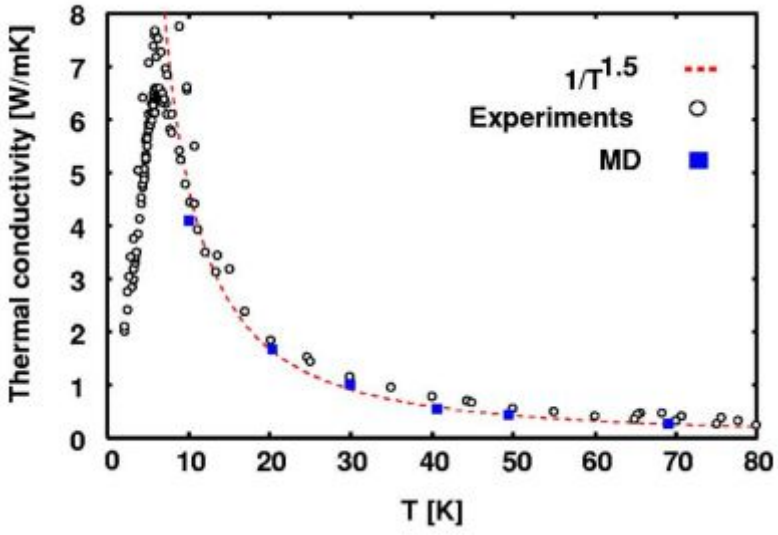

Figure 2-7 The heat conductivity data for molecular dynamics simulation and experiments as a function of temperature in the linear scale. [5]

Graphene is an allotrope of carbon in the form of planar sheets which are one atom thick with the atoms arranged in a honeycomb-shaped lattice, which has

been applied aiming to control heat flux in many electronic fields, such as, heat memory, heat logic gate, heat transistor and heat rectifier. [24] The heat conductivity of single layer graphene is observed to be up to 5300 W/(mK)[25], which is one order higher than some high heat conductivity materials, like copper. However, during the synthesis of graphene, defects, which may impact the thermal property of graphene, are inevitably induced in graphene. The heat conductivity of graphene decreases significantly with vacancy concentration using the Green-Kubo method (see section 4.8.2) in MD, especially at low concentration. (Figure 2-8) The shortening of mean free path is responsible for the initial rapid decrease of heat conductivity, whereas following slight drop in relatively high concentration results from the diffusion mechanism.[26]

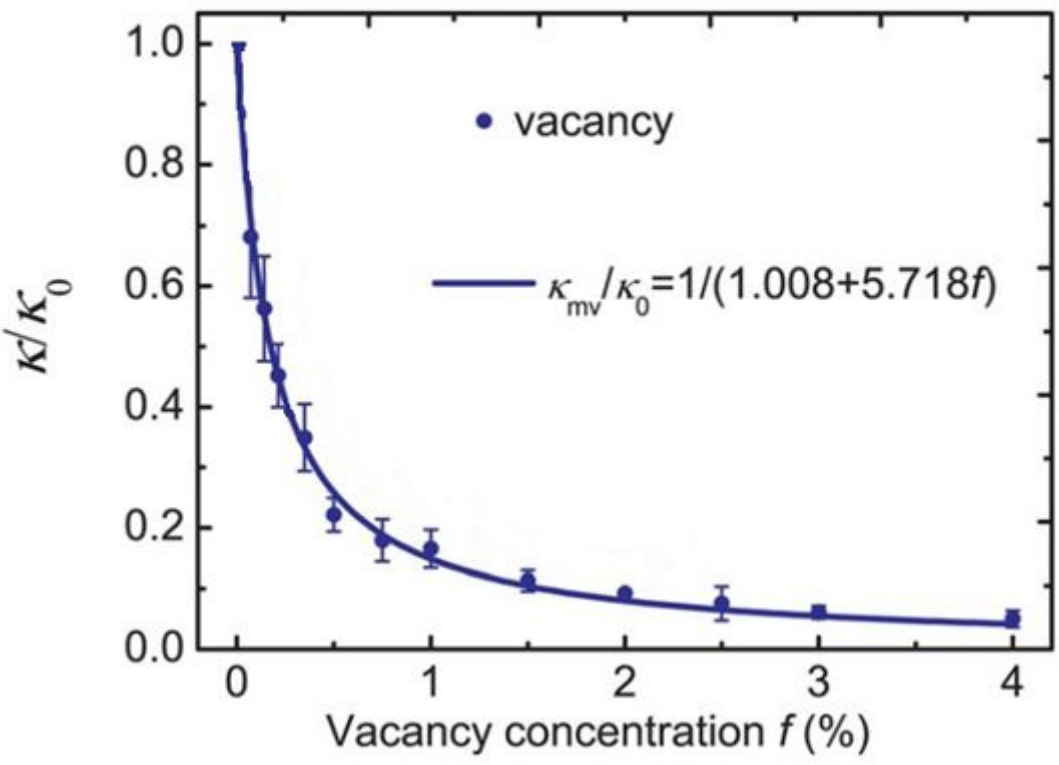

Figure 2-8 The heat conductivity of a single layer graphene with vacancies at 300 K. [26]

There are also other kinds of graphene analysed on heat transport in molecular dynamics, for example, asymmetrically **defected graphene nanoribbons** (**GNRs**)[27], parallel various-nitrogen-doped graphene[28](Figure 2-9) ,

triangular single-nitrogen-doped graphene[28](Figure 2-9), and armchair graphene nanoribbons induced by triangular vacancy[24](Figure 2-10). For asymmetrically defected graphene nanoribbons, a special phenomena has been found that heat flow has a preferable of direction. [27] They proposed optimum conditions for high heat rectifying efficiency of the heat rectifier proposed in their work. Furthermore, it is found that heat rectification of the single-nitrogen-doped graphene declines with the increase of temperature, while that of various-nitrogen-doped graphene stays still. [28] It is interesting that armchair graphene nanoribbons with triangular vacancy defects is used to study the heat conductivity. It may be guessed that heat conductivity has a huge reduction. Additionally, the most fascinating thing that the orientation of heat flux has a preferable choice is presented. [24]

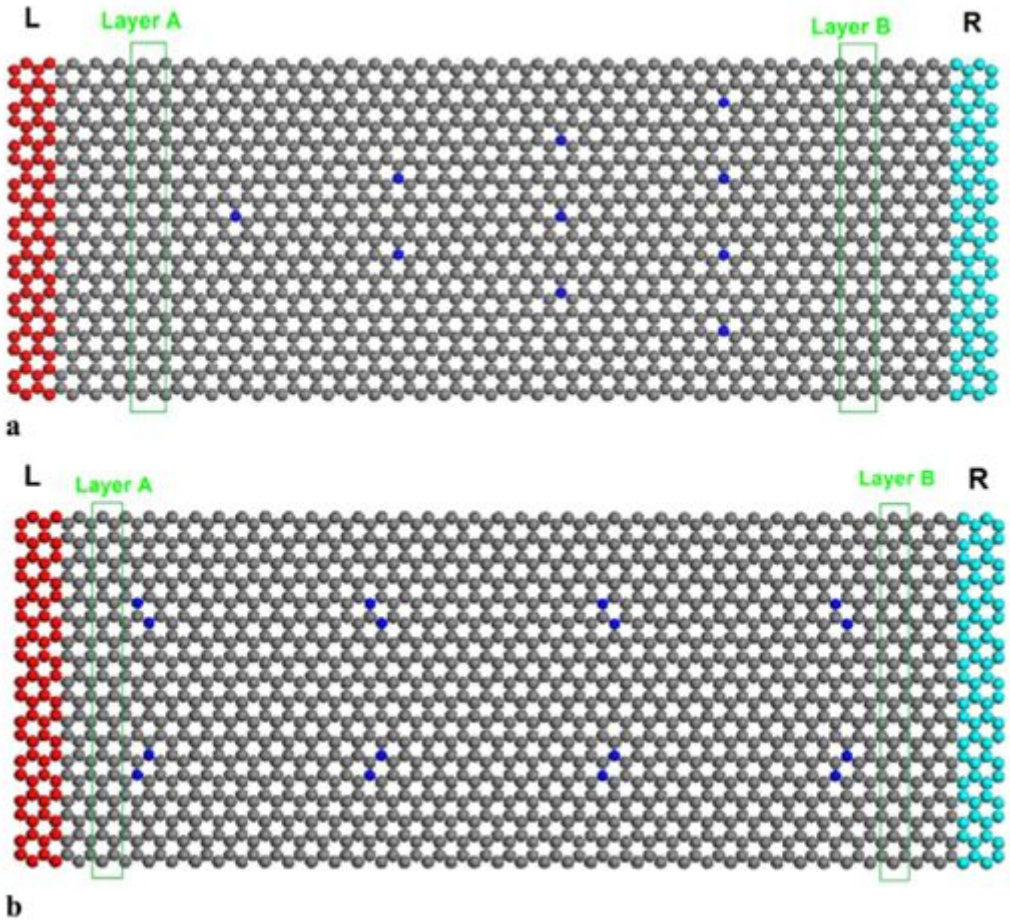

Figure 2-9 Two kind of nitrogen-doped graphene (NDG): (a) triangular single-nitrogen-doped graphene; (b) parallel various-nitrogen-doped graphene [28]

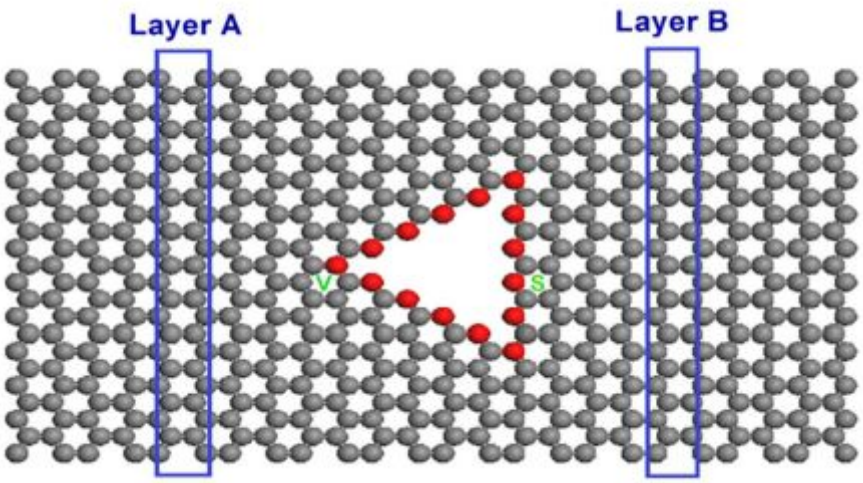

Figure 2-10 Armchair graphene nanoribbons with triangular vacancy defects. [24]

Si-based materials, such as silicon nanowires [29, 30] and silicon-germanium (SiGe) alloys [23], have been applied hugely in thermoelectric fields for their high value of the **figure of merit** (**ZT**), which is used to evaluate the efficiency of thermoelectric devices. The figure of merit is defined as,

$$ZT=S^2\sigma T/k \qquad \textbf{(2-1)}$$

where S is Seebeck coefficient, σ the electrical conductivity, T the absolute temperature, and k stands for heat conductivity. $S^2\sigma$ is called **power factor**, which plays a significant part in achieving high thermoelectric performance. [16]

As heat conductivity is inversely proportional to ZT [29], more concern should be put in reducing heat conductivity of Si-based materials for a high ZT value. Introducing vacancies in Si-based materials succeeded in lowering heat conductivity. [6, 31] As main medium of silicon is phonon, phonon heat conductivity attributes the major of heat conductivity. The phonon heat conductivity of silicon is proportional to the **phonon mean free path**. (see section 3.2.3) [31] The heat conductivity of silicon goes down non-linearly with defect volume fraction. And vacancies have a worse effect on heat conductivity than **vacancy nanovoids** (groups of atoms belonging to the same sphere) on condition of the same defect volume fraction. (Figure 2-11)[6]

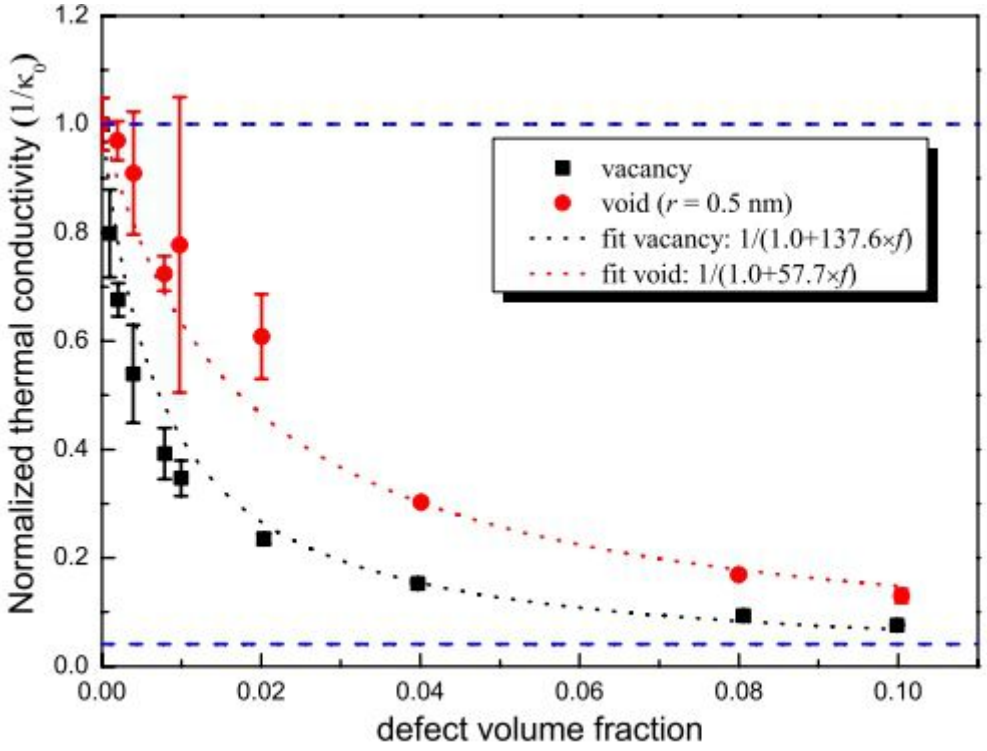

Figure 2-11 Normalized heat conductivity of silicon as a function of defect volume fraction. The values are normalized by perfect silicon heat conductivity at 500K. [6]

2.3.2 Metals

For metals, at the present moment, there is no appropriate molecular dynamics simulation to describe the total heat conductivity, because in MD atoms are thought as hard spheres and electronic structure is not considered. Under the circumstances of neglecting electrons, one would study the phonon heat conductivity of metals. **NEMD method** (see Section 4.8) has been proven to be an applicable way to calculate phonon heat conductivity in aluminium [32] and nickel [33]. Seven metals, which consists of Cu, Ag, Pt, Au, Pd, Ni and Ta, are used to calculate phonon heat conductivity by the direct method (NEMD method). In this case, the resulting conductivity values are much less than experimental data owing to the less consideration of electrons. [34]

The phonon heat conductivity of Cu, which was calculated by the Green-Kubo method, is of the same order of magnitude with that associated by the direct method. [34-36] The phonon component in the total heat conductivity is

relatively small, both in bulk metal and metallic films. [36] Compared with the experimental data, 0.5% and 10% of heat conductivity of bulk copper are attributed by phonons at 1300 K and 90 K respectively. [35]

The phonon heat conductivity of copper films rise with the film thickness. (Figure 2-12) In other words, the greater the thickness of copper film is, the greater the ratio (phonon heat conductivity of copper film to that of bulk copper) is. In addition, a magnificent thing has been found that the phonon contribution in copper films is enhanced by comparison with that in bulk copper. For example, the phonon heat conductivity of 10 nm (**nanometer**=10^{-9} m) thickness copper film accounts for around 3.76% of the total heat conductivity while phonon just attributes 2.16% of that for bulk copper at 475 K.[36]

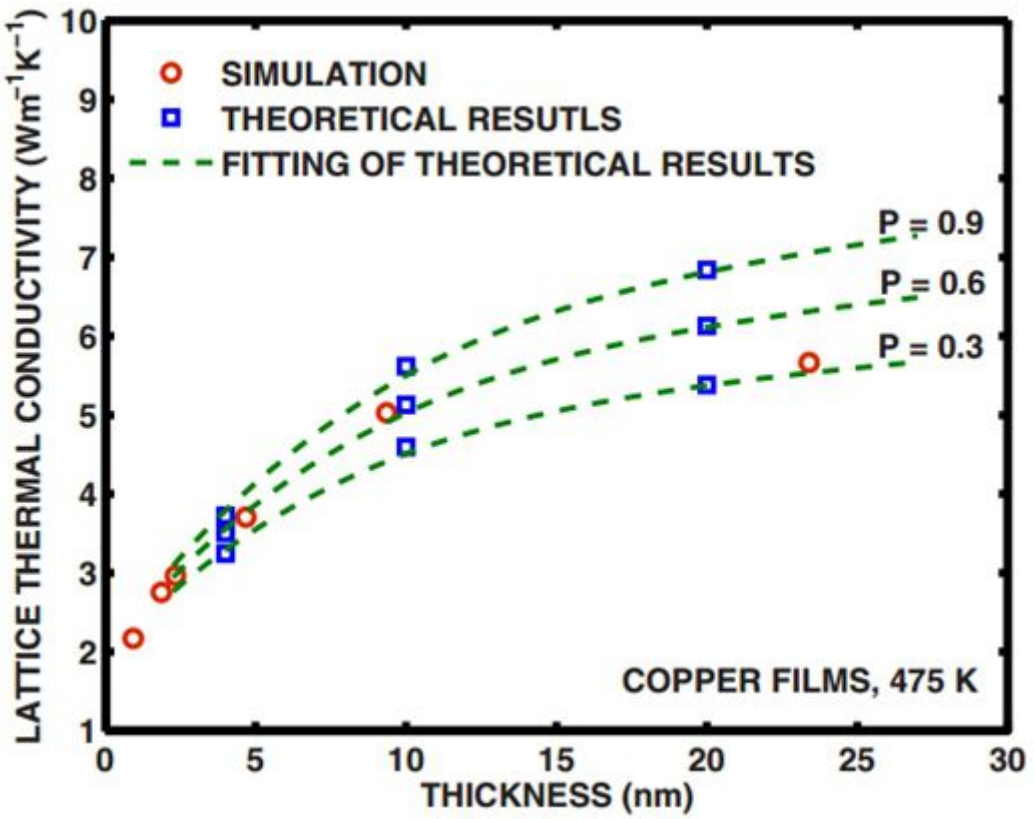

Figure 2-12 The phonon heat conductivity of copper films as a function of the film thickness at 475 K. P stands for surface roughness. P=0 corresponds to the totally diffuse surface while P=1 the totally specular surface. [36]

Regarding heat transfer of Cu, some researchers have studied the phonon heat conductivity of bulk Cu and film Cu. Nevertheless, until the present, there was no literature in studying the effect of defects on phonon heat conductivity in metals by means of MD.

2.4 Conclusions

This chapter briefly explores relevant literature about this work. In the beginning, it is proposed that heat exchangers, heat sinks and heat pipes are manufactured in order to cool devices. Cu should be taken into consideration in the process of finding appropriate materials for previous devices.

Then the review changes the direction to the possibility of effecting the heat conductivity of metallic materials. One method is to create defects in metals, the other one is to add a new element.

At last, the review presents the molecular dynamics study of heat conductivity in various materials. For non-metals and alloys, the review has mainly referred to investigations in which defects turn out to be harmful to phonon heat conductivity. However, the study range using MD method is limited to metals without defects.

Note that the above subjects are interconnected. First of all, heat pipes rely on high heat conductivity materials such as copper. A few studies about the effect of defects and alloy elements on heat conductivity have been mentioned. Regarding the MD method, the focus of researchers is to investigate the perfect metal. Nevertheless, for non-metals and alloys, there are a great number of studies about phonon heat conductivity, regardless of whether they are perfect. As mentioned previously, the MD simulation can only be implemented to understand the heat transfer contributed by phonons until now. Hence, the direction of the thesis is turned to how defects effect the phonon heat conductivity of copper. In this work, vacancy will be studied because it is the simplest defect.

3 Theory

This Chapter is illustrated in two parts, the fundamentals of crystalline solids and theory about heat transfer. The first part is related to the crystal structures, crystal defects. In particularly, the Face Centred Cubic (FCC) structure and vacancy are described in details. In the second part, the thesis provides a description about three modes of heat transfer, heat conduction, heat convection and heat radiation. Moreover, the major part is dedicated to heat conduction of solids.

3.1 Fundamentals of Crystalline Solids

Crystals are solids whose atoms or molecules are arranged in a highly structured and organised manner. Basing on the structures of the solids, they are divided into two broad categories, **crystalline solids**, those with a highly regular arrangement of their components, and **amorphous solids**, those with considerable disorder in their structures. [37]

3.1.1 Crystal Structure

The positions of the components in a crystalline solid are usually represented by a **lattice**, a three-dimensional system of points designating the positions of the components (atoms, ions, or molecules) that make up the substance. The smallest repeating unit of the lattice is called the **unit cell**.

The first thing we should do is to define a coordinate system, before describing the lattice. From Figure 3-1, a coordinate system is composed of three axes, x, y and z with inter-axial angles α, β, γ. The inter-axial angle α, β, γ is used to describe the angle formed between axes y and z, x and z, x and y, respectively.

The distance along the x axis from the **origin** (the intersection among three axles x, y, z) to the edge of the unit cell is called the **lattice translation vector**, **a**. The two other lattice translation vectors **b** and **c** are defined similarly. The magnitudes (lengths) of the lattice translation vectors are called the **lattice parameters** or **lattice constant**, a, b and c. By combination of lattice translation

vectors, 14 kinds of lattices are obtained, which are named Bravais lattice as a whole. [38] These are shown in Figure 3-2.

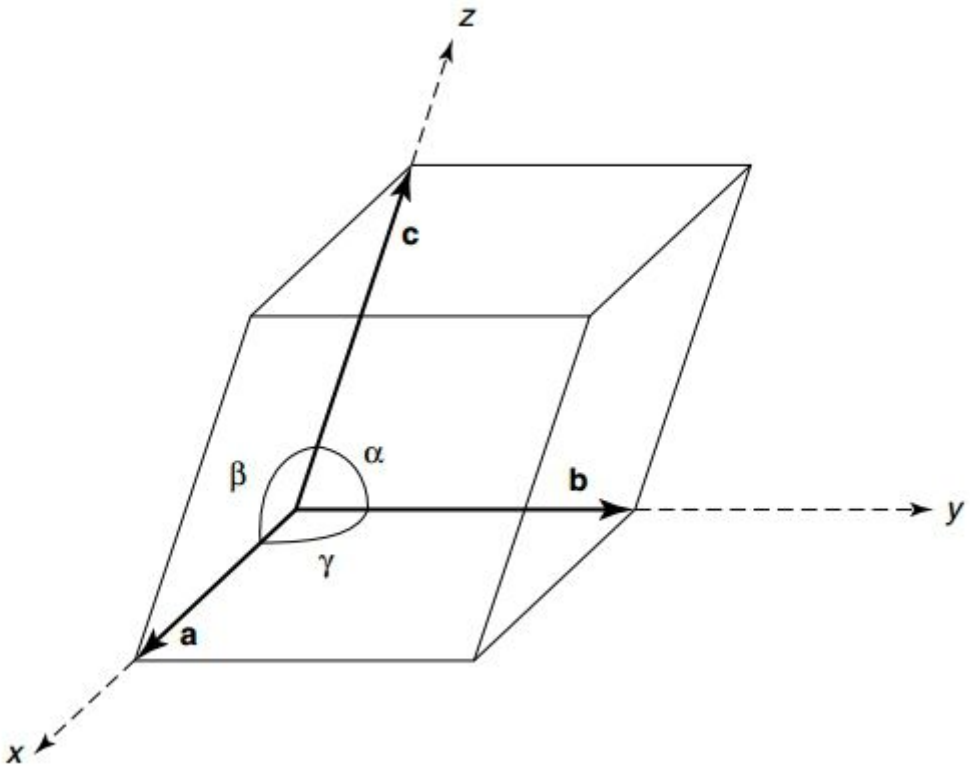

Figure 3-1 A simple coordinate system with three axes, x, y, z and three inter-axial angles, α, β, γ. [38]

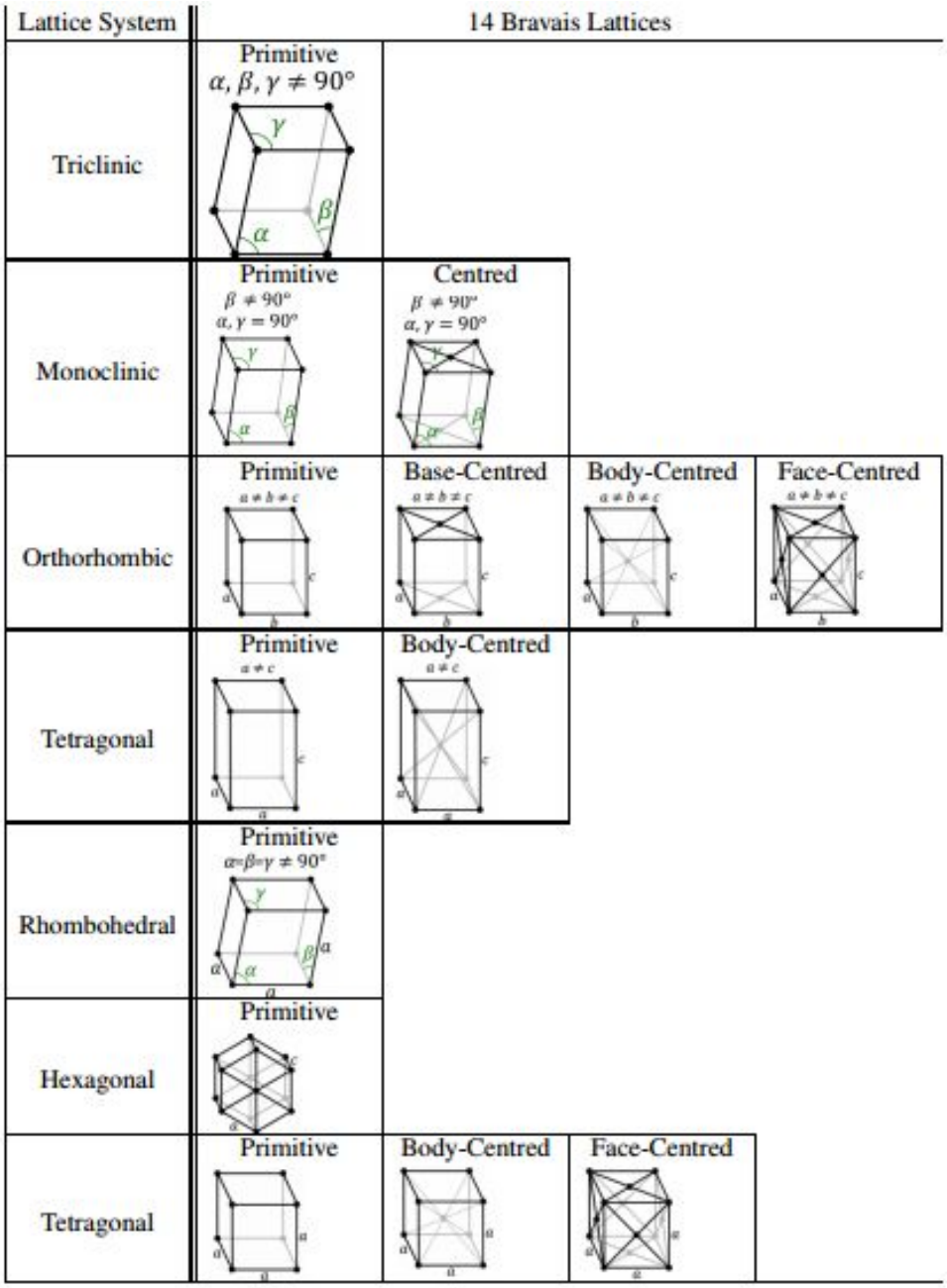

Figure 3- 2 The 14 Bravais lattices divided into 7 lattice systems [67]

However, for metals, Face Centred Cubic (FCC), Body Centred Cubic (BCC) and Hexagonal Close Packed (HCP) (see Figure 3-3) are employed commonly. In FCC structure, atoms are set at the corners and centre of each cube face of the unit cell. In BCC structure, atoms are located at the corners and the centre of the cube. The last one, HCP, has three planes of atoms. In the top and bottom plane, there are six atoms that arrange themselves in the shape of a hexagon and another atom that sits in the centre of the hexagon. The middle plane has three atoms situated at interstices of hexagonal planes.

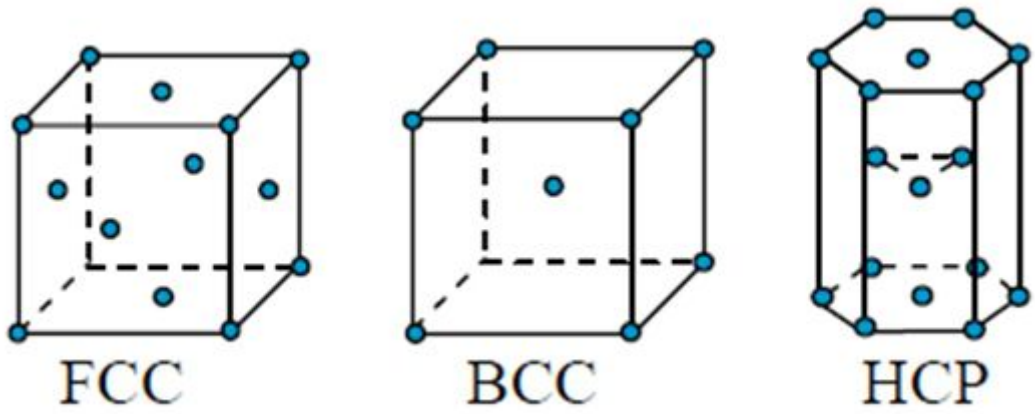

Figure 3-3 The unit cell of FCC, BCC and HCP

Face centred cubic is of interest due to it is the structure of Cu. Figure 3-4 illustrates that the centre atom is encompassed by six atoms in such a close manner, the plane of which is called **close-packed plane**. The layer of atoms shown in Figure 3-4 is labelled A. The next layer can be put above A in two different ways, B and C. For FCC structure, the stacking sequence is ABCABCABC...type. (Figure 3-5(a)) Figure 3-5(b) shows an FCC unit cell on the upper left area. The crystal structure type of many metals, such as, Cu, Al, Au and Ni, is FCC. [39]

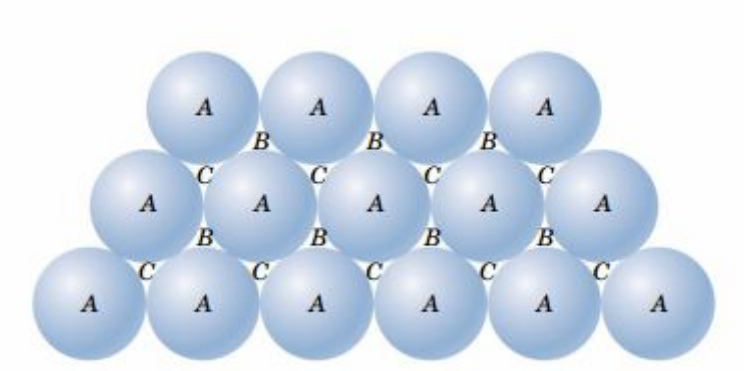

Figure 3-4 Close-packed plane A and two packing position B, C. [39]

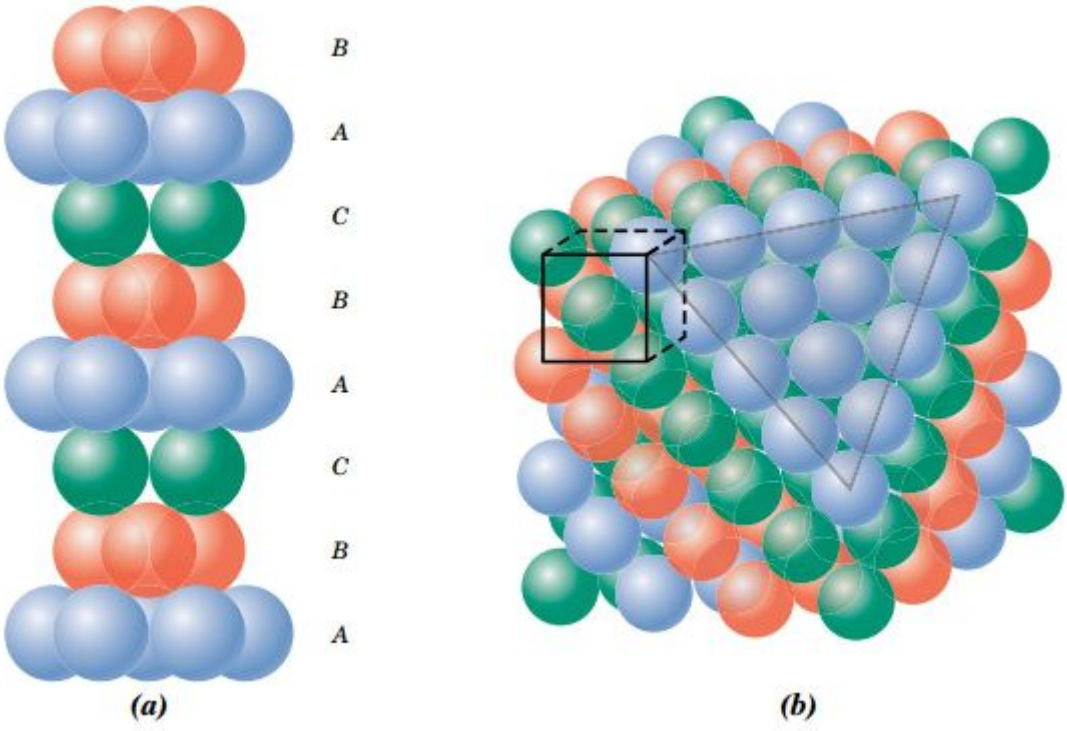

Figure 3-5 (a) stacking sequence of close-packed plane for FCC; (b) a schematic picture of describing the relation between FCC crystal structure and stacking of close-packed planes. [39]

3.1.2 Vacancy

In the real world, most of crystalline materials are imperfect, which contain all kinds of imperfections or defects. **A crystalline defect** is defined as a lattice irregularity having one or more of its dimensions on the order of an atomic diameter. Based on the geometry of the defect, it is classified into **point defects** (those associated with one or two atomic positions), **linear** (or one-dimensional) **defects** and **planar** (or two-dimensional) **defects**. This thesis focuses on point defect.

There are two types of point defect, namely a **vacancy** (or **vacant atomic site**) and a self-interstitial atom (see Figure 3-6), in a pure metal. A vacancy is a defect where an atom is missing compared to the crystal's perfect form. It is the simplest form of point defect. A **self-interstitial** is an atom from the crystal that is crowded into an **interstitial site**—a small void space that under ordinary circumstances is not occupied.

As the atom is substantially larger than the place where self-interstitial atom is arranged, a self-interstitial can introduce relatively large distortions in the lattice. In other words, the formation of a self-interstitial needs relatively much energy. Consequently, the formation of it is not highly probable, and the concentration of interstitial is smaller than that of vacancy. The concentration of self-interstitial on pure metals may be neglected compared with that of vacancy. [39, 40] Vacancies exist widely in all crystalline materials, as perfect crystals are almost impossible to manufacture. In this thesis, vacancy is focused on.

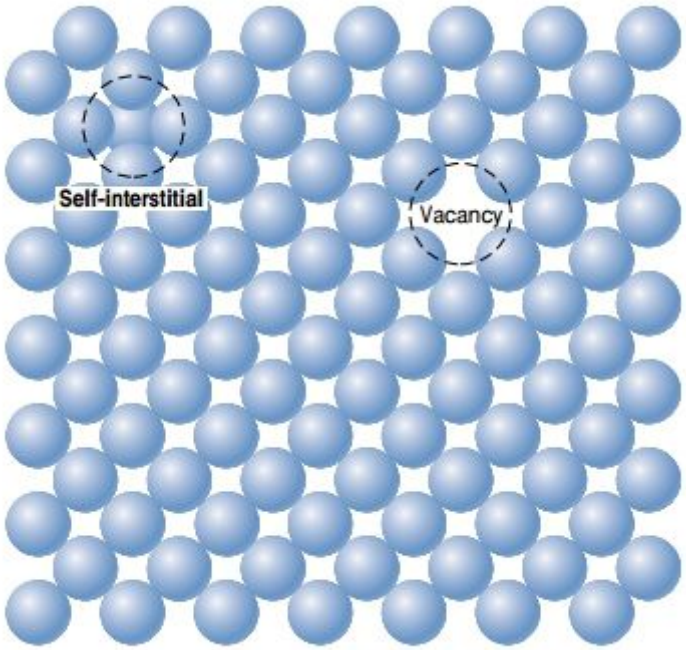

Figure 3- 6 Vacancy and self-interstitial [39]

3.2 Heat Transfer

3.2.1 Modes of Heat Transfer

Heat transfer is a process of describing how energy transfers between two parts of the same material or substances caused by the difference of temperature. Three heat transfer modes exist in nature, heat conduction, heat convection and heat radiation.

Figure 3-7 is the schematic diagram of three heat transfer types. Heat conduction is the transfer of energy between systems in contact in the presence of a temperature gradient. Heat convection is the transport of heat along with the mass of moving fluid. With regards to third mode, radiation, it is a process of creating net heat transfer by emitting energy in the form of electromagnetic waves between two surfaces at different temperature. [41]

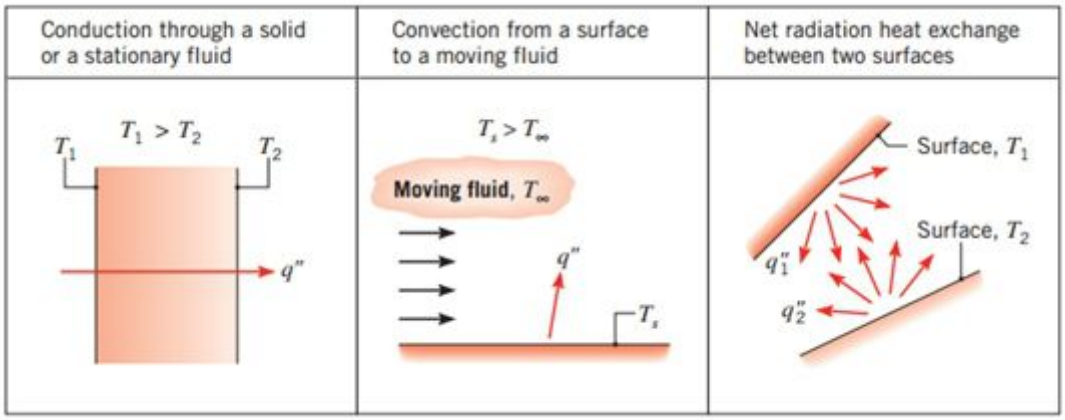

Figure 3-7 Three modes of heat transfer: heat conduction, heat convection and heat radiation from left to right. [41]

3.2.2 Heat Conduction

Conduction is a heat transfer mode that occurs when a temperature gradient exists in a material. The energy is transported from a higher temperature zone to lower temperature zone owing to the movements of atom or molecule.

Figure 3-8 shows the process of heat conduction by gas. In this case, we assume that there is no gravity effect. The particles close to the hot wall get energy from it and transport energy to other particles in the right through collisions and diffusion. The energy is transported continuously from the hot wall to the cold wall until they have the same temperature. [42] The situation is much the same in liquids, although the molecules are more closely located and they interact stronger with each other. In solids, where the motion of the atoms is restricted, energy is often transferred through **lattice vibrations**, called **phonons**. However, in metals, delocalized electrons also move across atoms transferring heat. [42]

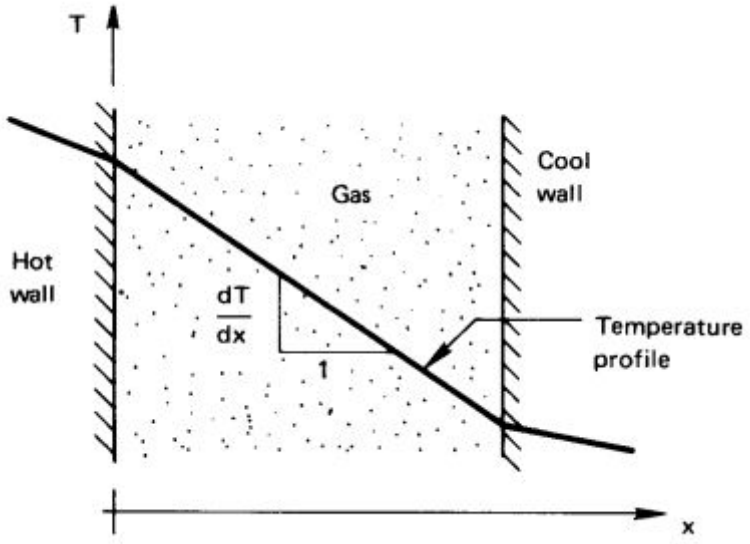

Figure 3-8 Heat conduction by gas. [42]

The simplest steady heat conduction problem is that of heat conduction across a plane wall with two different temperature faces (see Figure 3-9). The heat flows from the face with temperature T1 to the reverse face with T2. The heat transfer rate by heat conduction as Fourier's law is given by,

$$q=-kAdT/dx \quad \textbf{(3-1)}$$

Where q is heat transfer rate (W), k is heat conductivity of the materials (W/mK), A is cross-sectional area of heat path (m^2) and dT/dx is temperature gradient (K/m)

The heat transfer rate is proportional to the temperature gradient, by contrast, heat conductivity is inversely proportional to the temperature gradient.

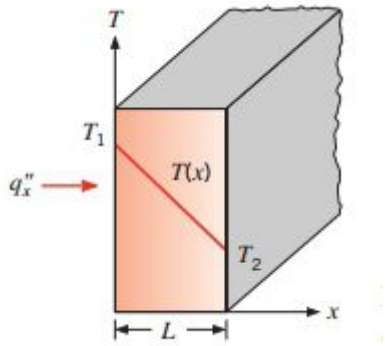

Figure 3-9 Heat conduction of two different temperature faces. [41]

Table 3-1 shows heat conductivity of some materials at 0 ℃. Generally, non-metals conduct heat worse than metals, and amorphous materials conduct heat worse than crystalline ones (crystalline materials have well-defined lattice structure than amorphous ones). Some solids, which are dry and porous, are great insulation.

Table 3-1 Heat conductivity of varied materials at 0 ℃ [44]

Material		Heat Conductivity k (W/mK)
Metals	Silver(pure)	410
	Copper(pure)	385
	Aluminum(pure)	202
	Nickel(pure)	93
	Iron(pure)	73
Nonmetallic Solids	Quartz, parallel to axis	41.6
	Sandstone	1.83
	Glass, window	0.78
Liquids	Mercury	8.21
	Water	0.556
Gases	Hydrogen	0.175
	Helium	0.141
	Air	0.024
	Water vapor(saturated)	0.0206

3.2.3 The Heat Conductivity of Solids

Heat transfer involves the transport of energy from a hotter area to a lower area by heat carriers. In solids, **phonons** (**a quantum of lattice vibration energy**) [45] or electrons are heat carriers. .

The heat conductivity is expressed by in kinetic theory,

$$k=1/3(Cv\lambda_{mfp}) \quad \textbf{(3-2)}$$

C is the specific heat per unit volume, v is the mean velocity, and λ_{mfp} is the mean free path of the particles (i.e. electron, phonon). In any case, the heat conductivity grows as the mean free path of the heat carriers (electrons or phonons) is increased. [41]

In solids, the heat conductivity may be presented by,

$$k=k_e+k_{ph} \quad \textbf{(3-3)}$$

Where k_e is heat conductivity contributed by electrons and k_{ph} is that by phonons. [41]

Initially, to an approximation, k_e is inversely proportional to the electrical resistivity, ρ_e. In pure metals, which have low ρ_e, electrons are main medium of heat conduction, whereas in non-metals, the phonon contribution to heat conduction heat transfer dominates. For alloys, the electrical resistivity of which are larger than pure metals, the donation of phonons can been not neglected any longer. The well-ordered arrangement of the lattice has a vital impact on phonon heat conductivity. For instance, quartz (crystalline material) has a higher heat conductivity than glass (amorphous material). Figure 3-10 expresses the temperature dependence of metallic and non-metallic solids.

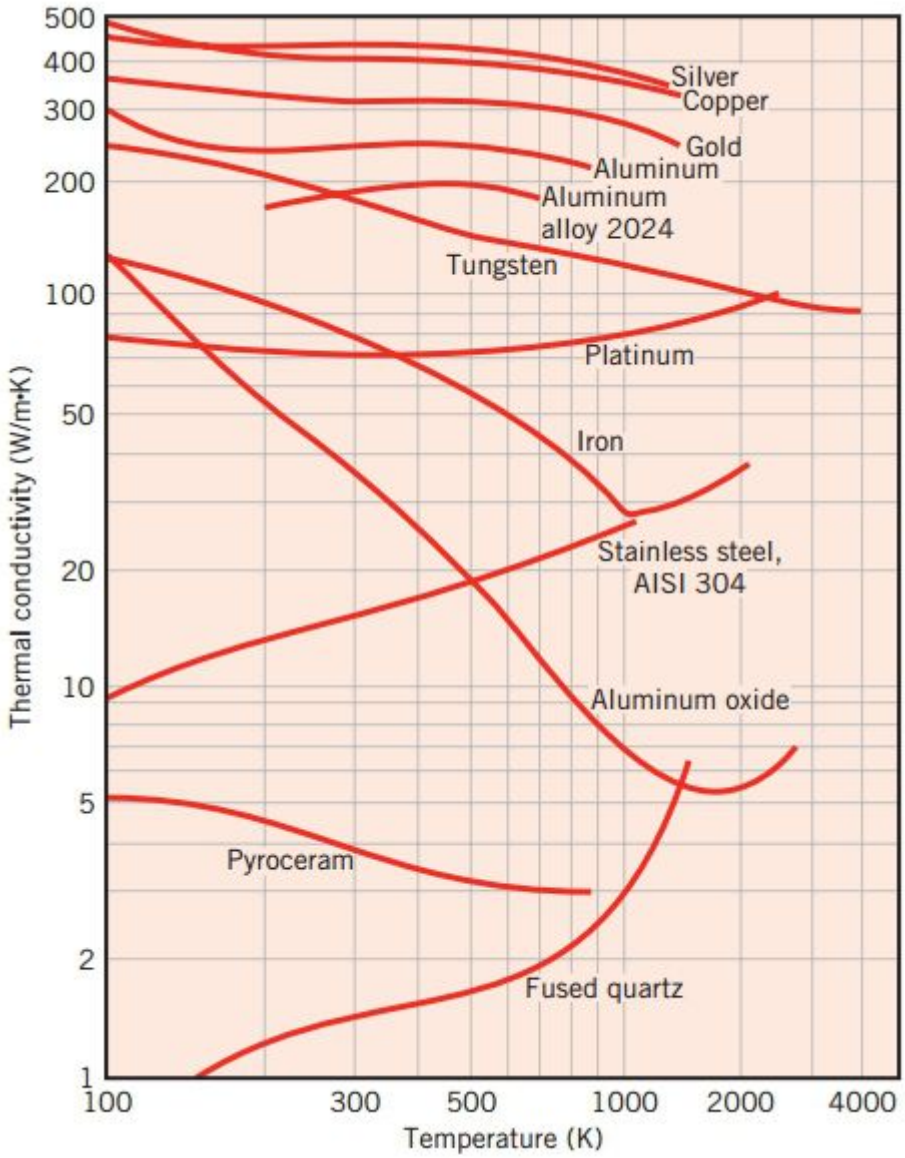

Figure 3-10 A picture of heat conductivity of many solids as a function of temperature. [41]

The previous description of this section is all about the bulk materials. In the following part, we will study the modification of heat conductivity of materials with a smaller dimension on the order of micrometers or nanometers.

Figure 3-11 presents two cross section of films of the same material with the thickness, L1 and L2, respectively. For a smaller λ_{mfp}/L (λ_{mfp}/L, namely **Knudsen number**, is a dimensionless number. Large Knudsen numbers suggest potentially remarkable nano- or microscale effects), the boundaries of film has a minor impact on diminishing the average energy carrier path length and the

heat is transferred the way like bulk material. (Figure 3-11 (a)) Nevertheless, with the decrease of film thickness, the boundaries of the material can reduce the average net distance travelled by the energy carriers. (Figure 3-11 (b)) Furthermore, the movements of energy carriers (electrons and phonons) in x direction are effected by the boundaries worse than that in y direction. Accordingly, it is found that $k>k_y>k_x$. (k, k_y and k_x represent the bulk heat conductivity of the film material, the heat conductivity of the film material in y direction and that in x direction, respectively)

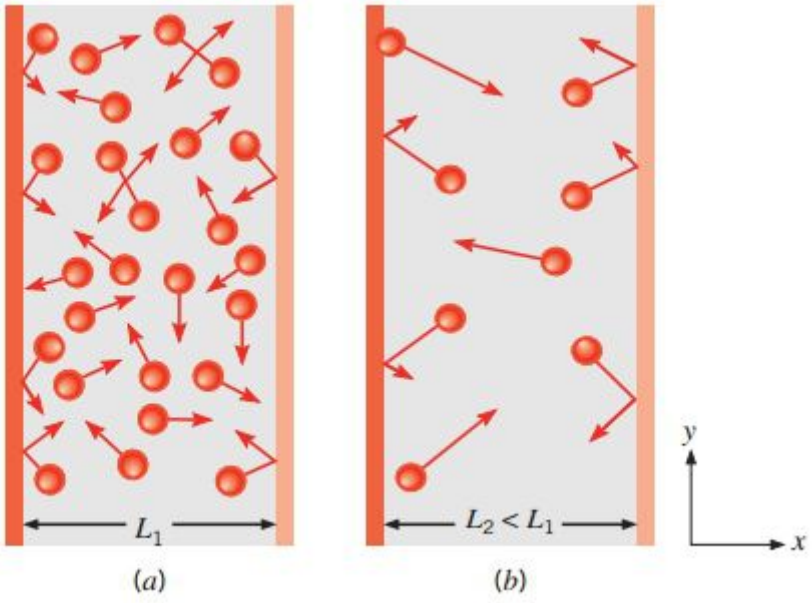

Figure 3- 11 Energy carriers trajectories in two films with the thickness L1 (a) and L2 (b). (L2 < L1)[41]

Except the scattering from the physical boundaries, energy carriers can be redirected by **grain boundary** (that is a region separating two grains or crystals of the same phase in a solid crystalline material) [46] or **dopant** that is a trace impurity element that is inserted into a substance. In other words, there is possibility to affect the heat transport for any kind of defect of materials.

4 METHODOLOGY

With rapid development of computer technology, computer simulation techniques, such as Monte Carlo (MC) and Molecular Dynamics (MD), have been widely used for understanding the microscopic phenomenon of materials. The greatest difference between them is that a new configuration is generated randomly for MC, while that is calculated by Newton's equations of motion. [47] In this thesis, MD is of my interest.

In this chapter, we introduce some basic concepts of molecular dynamics, as well as related techniques applied within the thesis. In the beginning, an introduction is made to general process of molecular dynamics simulation. After that, the main aspects of molecular dynamics, such as potential functions, the numerical method of integrating the Newton's equations of motion, boundary conditions and ensembles, are given information in details. Lastly, the rest of this chapter is dedicated to two common models of calculating the heat conductivity in molecular dynamics, the direct method and the Green-Kubo method.

4.1 Molecular Dynamics

The common procedure of molecular dynamics is shown in Figure 4-1.

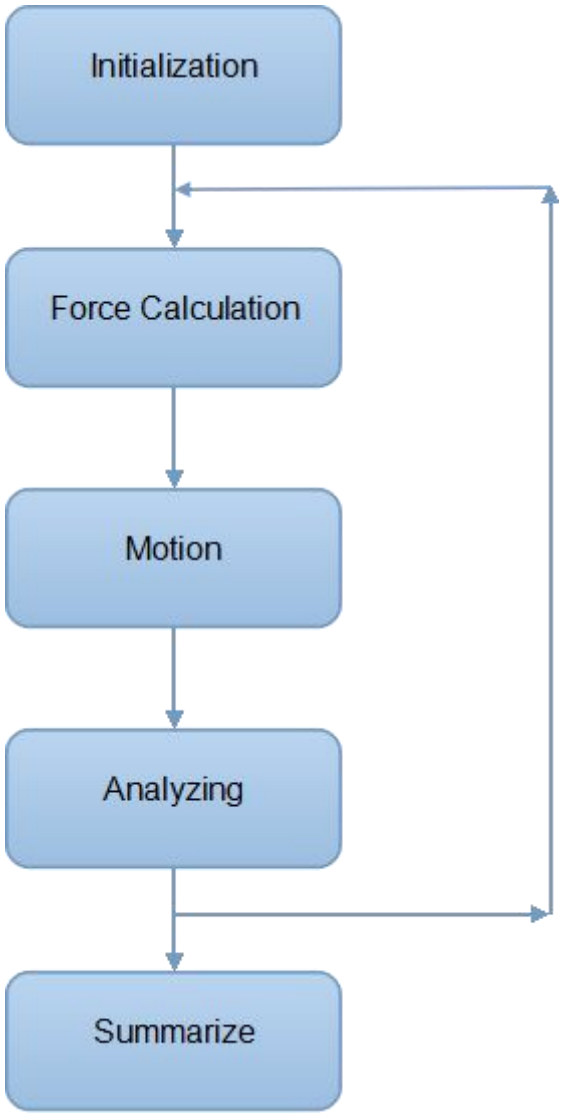

Figure 4-1 A schematic graph of general Molecular Dynamics process.

In the first step, initialization, the positions of atoms and their velocities must be specified. Then next step is to calculate atomic forces, which is usually the most time consuming process. In a simple simulation, pair forces, which are the forces between atoms, are applied, the famous one of which is Lennard-Jones potential function. If N atoms exist in the system, there will be N(N-1)/2 pairs of atoms, which means that to perform a molecular dynamics simulation needs

N(N-1)/2 times of calculation. For simplicity of calculation, one concept, cut-off, is introduced in molecular dynamics. The force between two atoms is assumed to be zero, if the distance between them is longer than the cut-off distance. After the calculation of interatomic forces, the third step is to integrate the Newton's equations of motion to evolve the positions and velocities of the atoms in time. From this new configuration of the system, the forces are recalculated and new positions and new velocities are received again. The above cycled process is repeated in tens of thousands of time steps in a simulation until data is large enough for analysing. [48]

4.2 Potential

In molecular dynamics, potential functions are of much importance to describe the potentials of system. The potential functions are derived from the potential energy of the system. This can be given by

$$V = \sum_i V_1(r_i) + \sum_i \sum_{j>i} V_2(r_i, r_j) + \sum_i \sum_{j>i} \sum_{k>j} V_3(r_i, r_j, r_k) + \cdots \quad \textbf{(4-1)}$$

where V_1 is the potential energy of an atom due to an external field, V_2 and V_3 describes the interaction of two and three atoms.

As the use of V_3 needs much computing, it is rarely considered in computer simulations.

Once the potential energy is obtained, the force for every atom is expressed as

$$F_i = -\nabla_{ri} V \quad \textbf{(4-2)}$$

where i is an arbitrary atom, F is the force obtained from potentials and $\nabla_{ri}V$ is the gradient of the potential as a function of space.

4.2.1 Lennard-Jones Potential

In molecular dynamics, **Lennard-Jones potential function** (also referred to as the **LJ potential**, **6-12 potential**), which was first presented in 1924[49], is the most popular pair potential. LJ potential is expressed commonly as

$$\phi（r）=4\varepsilon\left[\left(\frac{\sigma}{r}\right)^{12}-\left(\frac{\sigma}{r}\right)^{6}\right] \quad \textbf{(4-3)}$$

where ε is the depth of the potential well, σ is the distance at which the potential energy between two particles is zero, and r is the distance between the particles. (Figure 4-2)

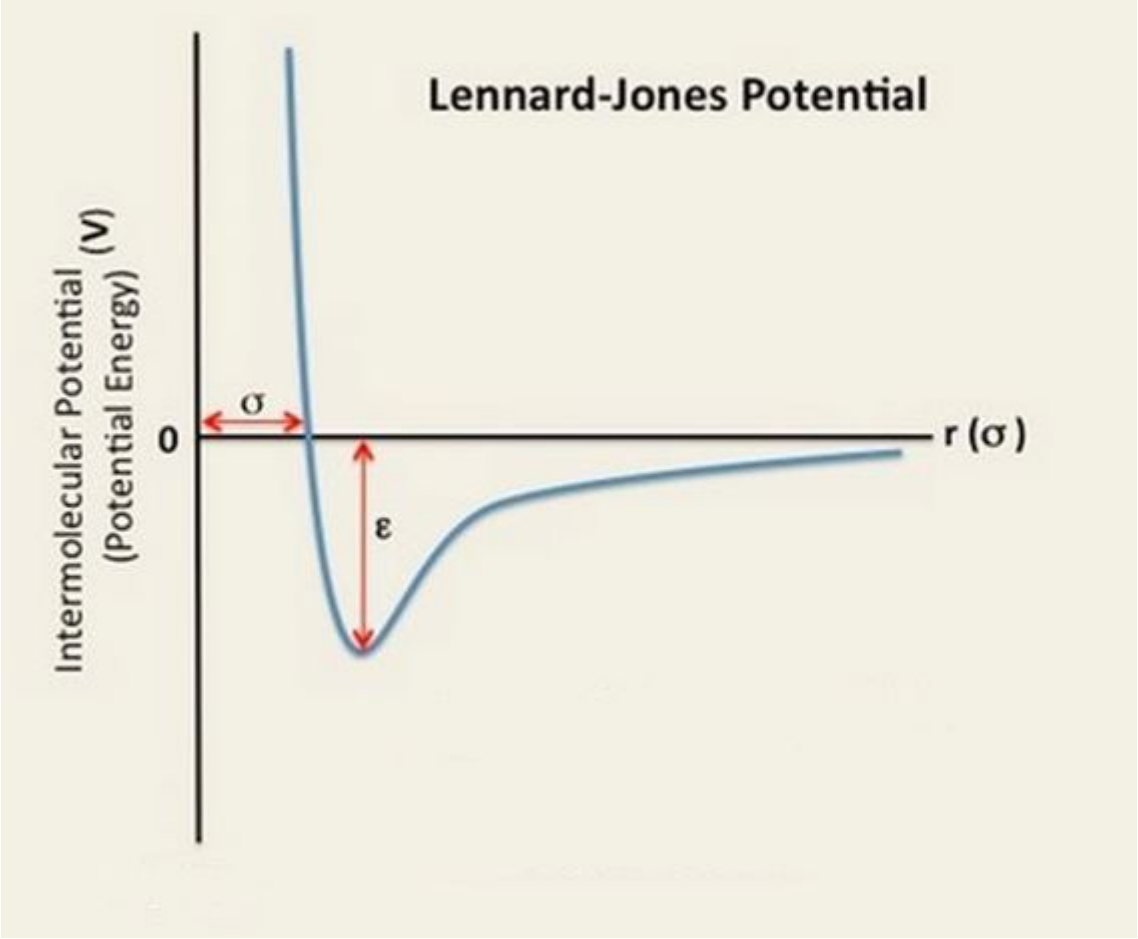

Figure 4-2 The L-J potential energy as a function of distance between two particles.

The L-J potential is a function of the distance between two particles. The first part of equation, $(\sigma/r)^{12}$ stands for the repulsive forces between two particles while the latter part of the equation, $(\sigma/r)^{6}$ denotes attraction. At long distances, the interatomic forces are attractive, while at short distances they are repulsive. The threshold between short and long is the distance when the potential reaches the minimum, -ε. Note that the deeper the well depth (ε), the stronger the interaction between the two particles.

The L-J potential is appropriate to describe simple non-bond interactions in some specific atoms, which are closed-shell atoms (Ne, Ar, Kr, etc.) and atoms that are fully coordinated. Also it can be applied together with some other potentials.

4.2.2 EAM

Embedded atom method (EAM) potential has become a powerful function in describing the interaction of two metal atoms in computer simulation. The original model is presented by and Mike Baskes and Murray Daw. [50] EAM potential induces an approximation to the many-atom interactions which is neglected by L-J potential, and can describe the physics of metallic bonding. [51]

Within the framework of density functional theory, the energy of a solid is a unique functional of the total electron density. In EAM potential, the total electron density in metals is approximated by the linear superposition of contributions from the individual atoms usually. The basic concept for EAM is that the potential energy can be calculated by embedding each atom to the electric field associated with all the surrounding atoms.

The total energy is expressed as [52]

$$E_{total} = \sum_{i} F_i(\rho_{h,i}) + \frac{1}{2}\sum_{i}\sum_{j(\neq i)} \phi_{ij}(R_{ij}) \qquad \textbf{(4-4)}$$

where R_{ij} is the distance between atoms i and j, Φ_{ij} is the short-range pair potential, $\rho_{h,i}$ is the local electronic density around atom i contributed from nearby atoms and F_i is the embedding function that represents the energy

required to place atom i into the electron cloud.

The electron density is expressed as,

$$\rho_{h,i} = \sum_{j(\neq i)} \rho_j^a (R_{ij}) \qquad \textbf{(4-5)}$$

where ρ_j^a is the electron density of atom j.

One of most important ways to identify sets of appropriate parameters of EAM is to fit them to cohesive energy, vacancy formation energy, bulk modulus, elastic constants, and so on. [52, 53] EAM has proven to be quite accurate in predicting bulk and surface properties of both pure metals and alloys. [52]

The Modified Embedded Atom Method (MEAM) developed by Baskes et al. [54] considers angular dependency of bonding on the base of EAM. With MEAM potentials can be calculated accurately in multi-component systems because of its wide range applicability of giving different interatomic potentials.

4.3 Integration

In the classical MD method, Newton's equations of motion are solved for atoms as, [55]

$$m_i \frac{d^2 r_i}{dt^2} = Fi \qquad \textbf{(4-6)}$$

Where m_i, r_i, F_i are mass, position vector, force vector of molecule i, respectively.

In MD, there are a variety of integration methods which differ in light of their different stability and accuracy. [56] Three most known are Verlet algorithm, Leap-frog algorithm and Velocity Verlet algorithm. The Verlet algorithm, which was proposed by Verlet in 1967 [57], is one of the most commonly methods to integrate Newton's second law (equation 4-6) in molecular dynamics.

In the Verlet algorithm, the position, velocities and accelerations can be approximated as Taylor Series expansions as:

$$r(t+dt) = r(t) + dtv(t) + \frac{1}{2}dt^2 a(t) + \frac{1}{6}dt^3 b(t) + \cdots \quad \textbf{(4-7)}$$

$$v(t+dt) = v(t) + dta(t) + \frac{1}{2}dt^2 b(t) + \frac{1}{6}dt^3 c(t) + \cdots \quad \textbf{(4-8)}$$

$$a(t+dt) = a(t) + dtb(t) + \frac{1}{2}dt^2 c(t) + \frac{1}{6}dt^3 d(t) + \cdots \quad \textbf{(4-9)}$$

$$b(t+dt) = b(t) + dtc(t) + \frac{1}{2}dt^2 d(t) + \frac{1}{6}dt^3 e(t) + \cdots \quad \textbf{(4-10)}$$

The new position r(t+dt) is obtained from the current position r(t), the current acceleration a(t) and the past position, r(t-dt). It is expressed as,

$$r(t+dt) = 2r(t) - r(t-dt) + dt^2 a(t) \quad \textbf{(4-11)}$$

where dt is the molecular time step.

In this scheme, it does not need the velocity to calculate the position. However, velocities can be used to compute the total energy, temperature, kinetic energy. Although velocity is not directly associated with the Verlet algorithm, it can be obtained by,

$$v(t) = \frac{r(t+dt) - r(t-dt)}{2dt} \quad \textbf{(4-12)}$$

4.4 Boundary Condition

Usually the simulation size of molecular dynamics is restricted to an upper limit due to the time and efficiency of computing. In a simulation, only a small sample of the system is modelled. **Periodic boundary condition (PBC)** is a trick for diminishing surface effects of simulation system. For example, in a 10×10×10 cubic system there are 1000 atoms, and about half of them present on six faces. The surface atoms equal 6 percent of the amount especially for 10^6 atoms.[58] The surface effects mainly have two hazards: the first, the atoms in or nearby the surface may leave the system in the process of molecular dynamics; the second, they are influenced by other atoms less than that in the centre of the

system. For eliminating surface effects, a term, called by periodic boundary condition, is introduced in simulation. Figure 4-3 illustrates the concept of PBC. The simulation cell of interest is replicated in 2 dimensions to form a two-dimensional space without boundaries, and atoms of replicated boxes have same positions and velocities. Whenever an atom leaves the simulation box, there must one image getting in it resulting the number of atoms in simulation box is conserved. If an atom is close to a boundary, it interacts with the atoms in the opposite side of the image through the boundary as long as the distance between them is within the cut-off radius (see Section 4.5).

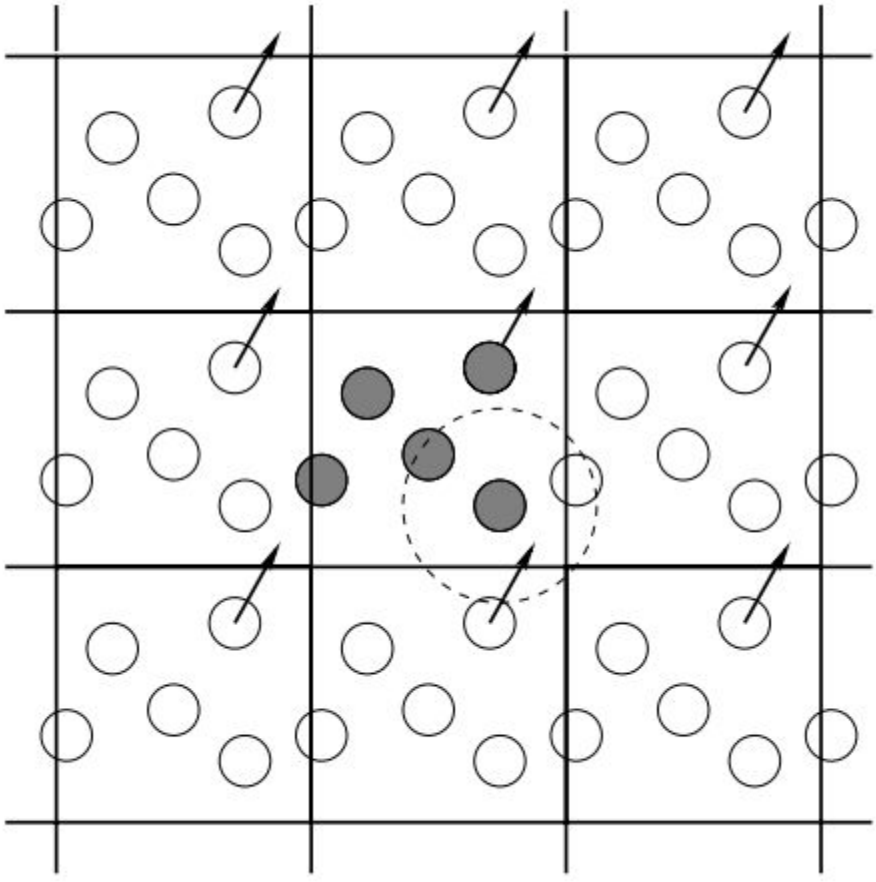

Figure 4-3 Periodic boundary condition. [58]

4.5 Cutoff

Another optimization technique in MD is the application of **cutoff radius** (a distance beyond which all interactions are disregarded). It is assumed that the potential between two atoms can be truncated beyond a certain distance r_c (cutoff radius). So the number of potentials that need to calculate decreases. For Argon, the common choice of cutoff radius is $r_c = 2.5\sigma$ [57], but for some specific purpose, other choices are used. For example, in a study of calculating the heat conductivity of Argon r_c equals four times of σ aiming to neglect the pressure correction. [41]

4.6 Ensemble

Statistical mechanics is the discipline that describes the physical phenomena in terms of a statistical treatment of the behaviour of large numbers of atoms or molecules. Statistical mechanics is of great use to link microscopic particle motion with macroscopic quantities.

A **microstate** is defined as a state of the system where all the parameter of the particles are specified. For a system specified in macroscopic variables (such as, E (energy), T (temperature) and N (number)), many microstates exist. An **ensemble** is a collection of all microstates of a system, consistent with the constraints with which we characterize a system macroscopically. For each atom, it is identified by position **r** and momentum **p** in 1, 2, 3 dimensions. For a system of N atoms, the position and the momentum will give it 6N degrees of freedom, and an arbitrary microstate are shown as the point ($\mathbf{r}^N$, $\mathbf{p}^N$).

There are several different kinds of ensembles that can be used in MD simulation, such as **microcanonical (NVE) ensemble**, **canonical (NVT) ensemble** and the **isothermal-isobaric (NPT) ensemble**. In this thesis, the NVE ensemble and NVT ensemble will be discussed. In NVE ensemble the system has constant particle number N, volume V and total internal energy E. It means any two microstates with the same N, V and E, have an equal probability of occurring. The uniform probability distribution is expressed as,

$$P_{NVE}((r^N, p^N)) = \frac{\delta(\mathrm{H}(r^N, p^N) - E)}{\sum_{micro} \delta(\mathrm{H}(r^N, p^N) - E)} \quad \textbf{(4-13)}$$

where H is the Hamiltonian defined as the sum of the kinetic and potential energy (for example, total energy of the microstate); N is the number of atoms in the system; E is the macroscopically dictated energy; and δ is the Kronecker delta given by

$$\delta(n) = \begin{cases} 1, n = 0 \\ 0, n \neq 0 \end{cases} \quad \textbf{(4-14)}$$

NVE ensemble is thermally isolated, so it is often used in the case that simulated system has no energy exchange with circumstance.

The NVT ensemble, called canonical ensemble, represents the possible microstates of the system in thermal equilibrium with a heat bath at a fixed temperature. (Figure 4-4) The total energy of the heat bath and the system is constant. The probability of finding the system in some microstate i with energy Ei is given by the Maxwell-Boltzmann distribution, which is defined as,

$$pi = \frac{e^{\frac{E_i}{k_B T}}}{\sum_i e^{\frac{E_i}{k_B T}}} \quad \textbf{(4-15)}$$

where k_B is the Boltzmann constant.

In NVT ensemble, the system can exchange energy with the heat bath for balancing conserved temperature.

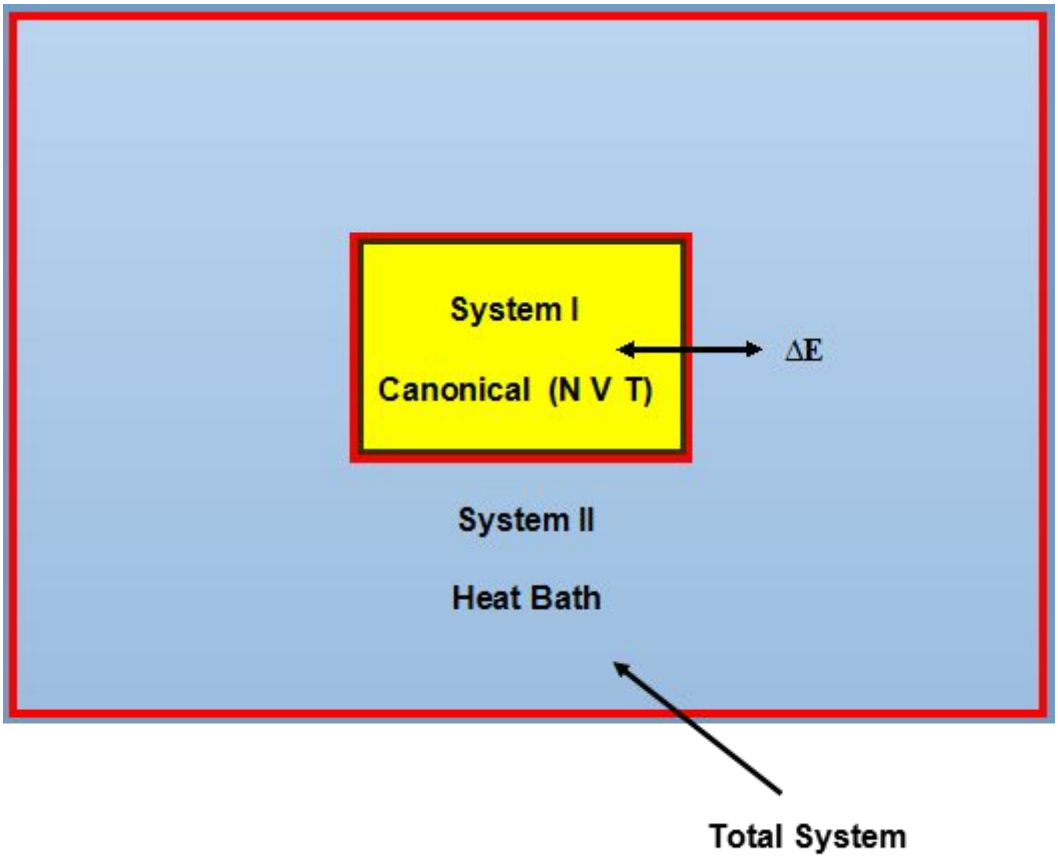

Figure 4- 4 A schematic of canonical ensemble (NVT)

4.7 Averaging

In MD simulation, the velocities and positions of atoms are measured in each instantaneous time, while the average macroscopic properties like pressure and temperature cannot be calculated accurately just using the instantaneous data. To derive useful data from the microscopic world, it is of necessity to build a bridge to link macroscopic properties with microscopic information. Statistical mechanics is a perfect choice to solve above problems. [59]

At any given time, a system of N particles can be described by a point in a 6N dimensional phase space Γ. **Phase space** has two components, a 3N dimensional configuration space and a 3N dimensional momentum space. The path through which the point in phase space evolves with time is called the **phase space trajectory**. So at a given time t, the positions and momenta of all

particles in the system correspond to a single point on the phase space trajectory. All the other properties computed in a MD simulation are a function of phase space. So these properties also evolve with time as the system passes along the phase space trajectory. For some property such as A (Γ(t)) which is a function of the phase space the instantaneous value is not a constant with respect to time. A is a fluctuating quantity with time and any measurement for this property should be done during a long enough period of time. So the time average for A is given by:

$$\langle A \rangle = \lim_{t\to\infty} \frac{1}{t} \int_0^t A(\Gamma(t))dt \qquad \textbf{(4- 16)}$$

where angled brackets denote the time average.[59]

4.8 Molecular Dynamics Study of Heat Transfer

Over the last decades, MD simulation has been applied widely in heat transfer. With the increasing capability of computer technology, more complex potential functions have been applied, no longer limited to the simple pair potentials, for example, Lennard-Jones.

As presented previously, heat transfer involves the transport of energy from a hotter area to a lower area by heat carriers. In solids, phonons or electrons are heat carriers. Nonetheless, to date, only the phonon heat conductivity can be calculated in molecular dynamics.

Two common methods of calculating heat conductivity in MD are the Green-Kubo method and the direct method. The Green-Kubo method, is an equilibrium molecular dynamics (EMD) method that obtains heat conductivity by the integral of heat current autocorrelation function. The other approach, the direct method, is a non-equilibrium molecular dynamics (NEMD) method that works by inducing a temperature gradient across the system.

4.8.1 The Direct Method

In generally, the NEMD method uses Fourier's law to calculate the heat conductivity. One way is to introduce the temperature gradient and measure the

heat that passes across the hot and cold region. The other is the direct method which exchanges kinetic energy and measure the temperature gradient to use it for Fourier's law.

In the direct method, velocities of particle are rescaling at every molecular dynamics timestep, the energy $\Delta\varepsilon$ is added in the hot region ($-L_z/4$ region) and removed from the cold region ($L_z/4$ region). (see Figure 4-5)

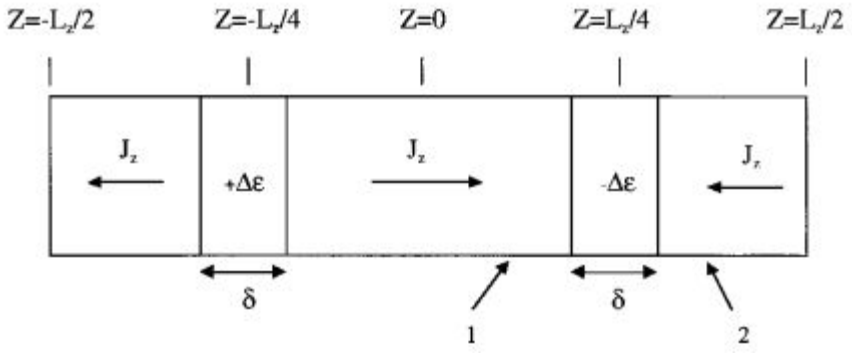

Figure 4-5 Schematic representation of the direct method [4]

After equilibrium state, the heat current (J_z) can be expressed as,

$$J_z=\Delta\varepsilon/(2A\Delta t) \quad \textbf{(4-17)}$$

Where A is the cross-sectional area, Δt is time of each step.

The temperature gradient is obtained, and at the end step, heat conductivity is gained by Fourier's law (Equation 3-1). [4]

4.8.2 The Green-Kubo Method

The Green-Kubo method, as an EMD simulation approach, is expressed by,

$$k=\frac{1}{3Vk_BT^2}\lim_{t\to\infty}\int_0^t\left\langle J_q(t')J_q(0)\right\rangle dt' \quad \textbf{(4-18)}$$

where k_B is the Boltzmann constant, V is the volume of the system, T is the absolute temperature, $\mathbf{J}_q$ is the microscopic heat current vector and t is the time, $\langle\mathbf{J}_q(t)\mathbf{J}_q(0)\rangle$ is **heat current autocorrelation function (HCACF)**, which measures how long it takes on average for phonons to dissipate.

The microscopic heat current vector is given by:

$$J_q = \frac{d}{dt}\left(\sum_i e_i r_i\right) = \sum_i e_i v_i + \sum_i r_i \frac{de_i}{dt} \qquad \textbf{(4-19)}$$

where the summation is over the atoms in the system, and e_i is the energy (kinetic and potential) of the i-th atom, $\mathbf{r}_i$ is the radius vector of the i-th atom and $\mathbf{v}_i$ is the velocity vector of the i-th atom.[60]

In a molecular dynamics simulation, **correlation length**, the total time for calculation of HCACF, must be long enough to ensure that the HCACF decays to zero. As phonon heat conductivity is the integral of the HCACF, the final result is not accurate if the HCACF does not drop to zero.

In materials where the mean free path of phonons is large, the HCACF decays slowly leading to a large integral of the HCACF. As the heat conductivity is associated with the integral of the HCACF, it is also high. [61]

The phenomena where HCACF presents a two-stage decay feature has been found in many materials.[5,35,66] The rapid decay corresponds to the partition of heat conductivity associated with short wavelength phonons, while the slow decay corresponds to the partition of that with long wavelength phonons.[61]

4.8.3 Summary

The heat conductivity of materials in molecular dynamics can be computed either by Green-Kubo method or by the direct method. However, the Green-Kubo method takes much more time in computing heat conductivity than the direct method. [4] Generally, the Green-Kubo method is more suitable to bulk material, whereas the other method is preferable for finite structures. [62] A significant advantage of the Green-Kubo method is that the whole phonon heat conductivity tensor can be computed in a model. On the contrary, the direct method needs several simulations in every direction in order to do the same. [65] Two methods have their advantages and disadvantages and there is no perfect one. Furthermore, the Green-Kubo method is applied in this work.

5 Validation of the Computational Model

This chapter describes the whole process of making a model associated with the phonon heat conductivity in MD method firstly. Then the model applied for investigating the phonon heat conductivity of copper without defects is validated in comparison with the data from other researchers.

5.1 Model

Here we introduce a brief MD model of pure Cu, which is used to gain the phonon heat conductivity. (Figure 5-1)

First, the structure of the system is defined. The system consists of 4000 atoms in a box with the dimensions of 10σ×10σ×10σ (**lattice constant**) along x [1 0 0], y [0 1 0] and z [0 0 1], respectively. The structure is a Face Centred Cubic (FCC) crystalline structure whose lattice constant (σ) is 3.615 Å. [52] Periodic boundary conditions is applied in all three directions (x, y and z).

Next step is to choose the potential function of the system. Embedded atom method (EAM) potential has been applied widely in molecular dynamics, due to its high accuracy of describing the interatomic interaction in metals. In this thesis, we choose Cu_u3.eam, which is presented by Foiles in 1986. [52]

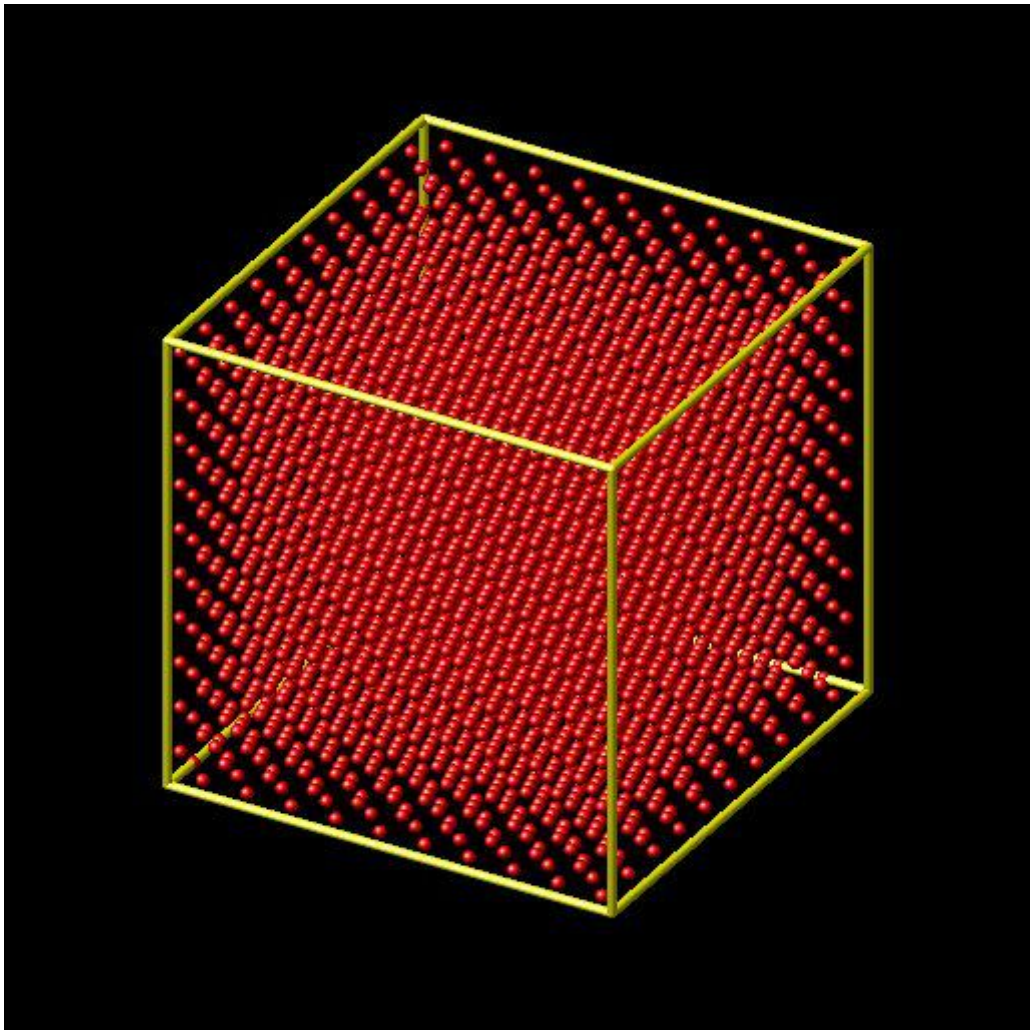

Figure 5-1 MD model of pure copper

With regards to the body of the model, there are two common types in calculating the heat conductivity. One of them is to put the system in canonical (NVT) ensemble firstly, and then in microcanonical (NVE) ensemble. At the first stage, the simulation is implemented in NVT ensemble for enough time to obtain a stable temperature of the system. At the second stage, the phonon heat conductivity is calculated by the Green-Kubo method in NVE ensemble for a longer time. The other one is to only settle the system in NVT ensemble. However, the computation of phonon heat conductivity cannot be started until the temperature of the system is stable. Not only in NVE ensemble and but also in NVT ensemble the phonon heat conductivity can be calculated accurately only if the temperature is stable. [35]

5.2 Validation

In this section, we validate the model implemented for acquiring the phonon heat conductivity of pure Cu at different temperatures.

5.2.1 The Model

The model is created based on the previous one (Section 5.1). The system is run first in NVT ensemble in 2 million timesteps, then it is put into the NVE ensemble in 10 million timesteps. The Green-Kubo method (see section 4.8.2) is used in molecular dynamics to get the phonon heat conductivity in every 100 K from 100 K to 1300 K. The reason that the maximum temperature is 1300 K is the melting temperature of Cu is 1357 K in experiments. The time step is 0.003 ps at 100 K, 0.002 ps at 200K and 0.001 ps for other temperatures. The correlation length of HCACF is 20000 time steps.

5.2.2 Results

In order to validate the model, the first factor to take into consideration is whether or not the total simulation time allows for the convergence of the phonon heat conductivity. In principle, in the Green-Kubo approach the total simulation time should be infinite long [63] which is of absolutely impossibility. For any simulation with a finite time, the time length is directly related to the accuracy of the computation of phonon heat conductivity.

Take the model at 300K for example, Figure 5-2 plots the phonon heat conductivity of pure Cu at 300K calculated in three direction x, y and z axle as a function of the number of timesteps. In the beginning, the phonon heat conductivity moves dramatically until the time reaches about 4 million timesteps, and then it keeps stable.

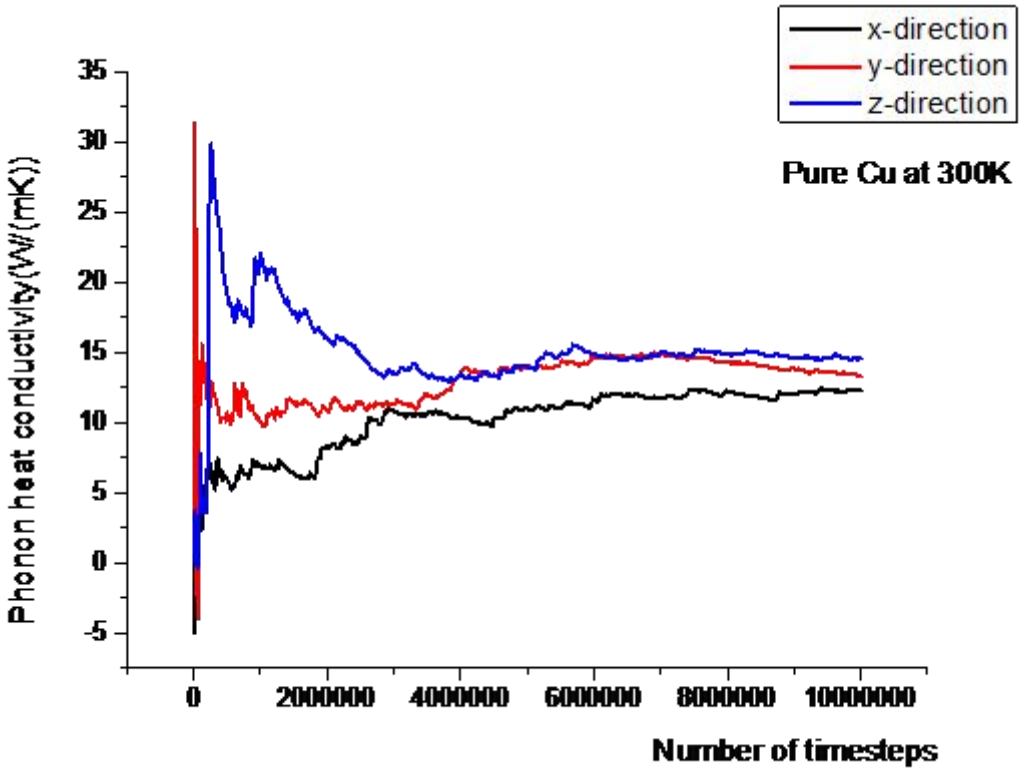

Figure 5-2 The phonon heat conductivity of pure Cu at 300 K in x, y, z direction with time.

If the simulation time is less than 4 million timesteps, the result of it is definitely inaccurate. As is presented in Figure 5-2, this model has a great convergence.

Next we discuss the value of phonon heat conductivity. Blue plots in Figure 5-3 presents the phonon heat conductivity of pure Cu obtained in different temperatures, and red plots demonstrates other researcher's results (which were obtained by the Green-Kubo method) [35]. By comparison, our results have the same order of magnitude with the data (Figure 5-3). It presents that phonon heat conductivity decreases with temperatures as well. The choice of EAM potential function probably gives rise to the difference of values between them.

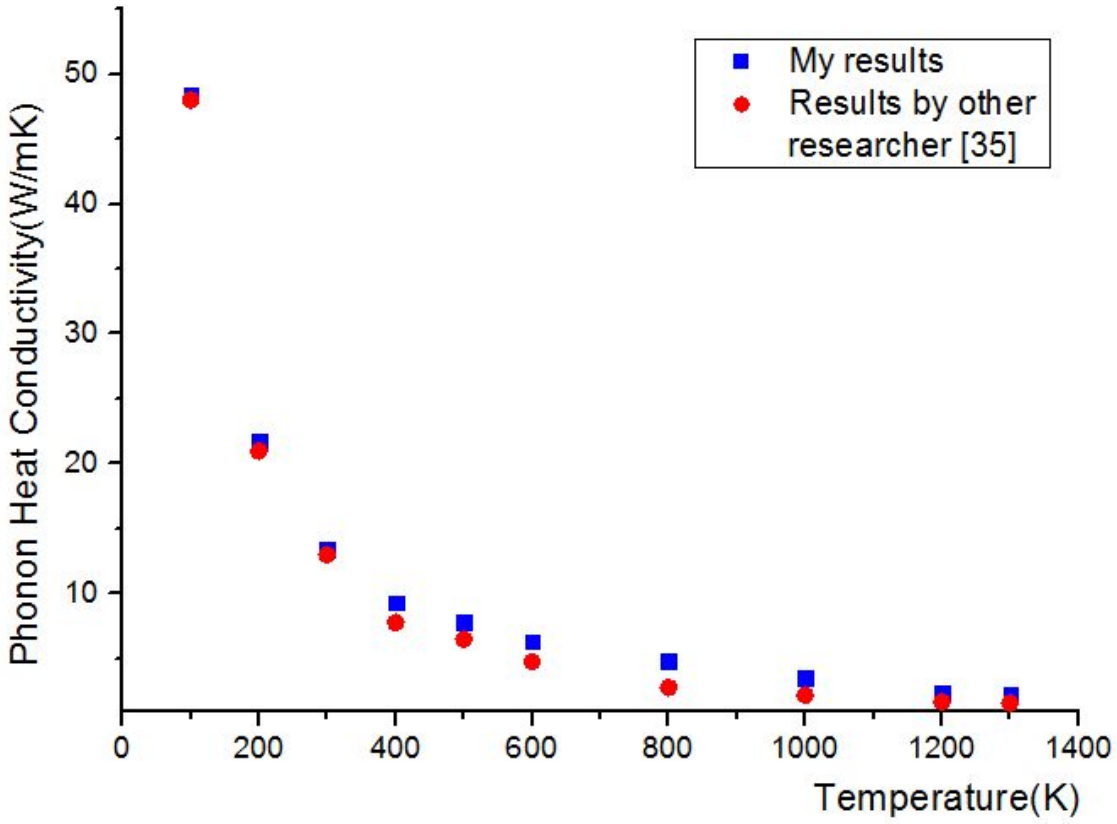

Figure 5-3 The phonon heat conductivity of pure Cu as a function of temperature： (1) blue plots (my results); (2) red plots (results by other researcher) [35]

The total heat conductivity is consisted of electronic heat conductivity and phonon heat conductivity, which are contributed by electrons and phonons, respectively. The ratio of phonon heat conductivity to total heat conductivity decreases from about 10% at 100 K to about 0.7% at 1200 K. (Figure 5-4)

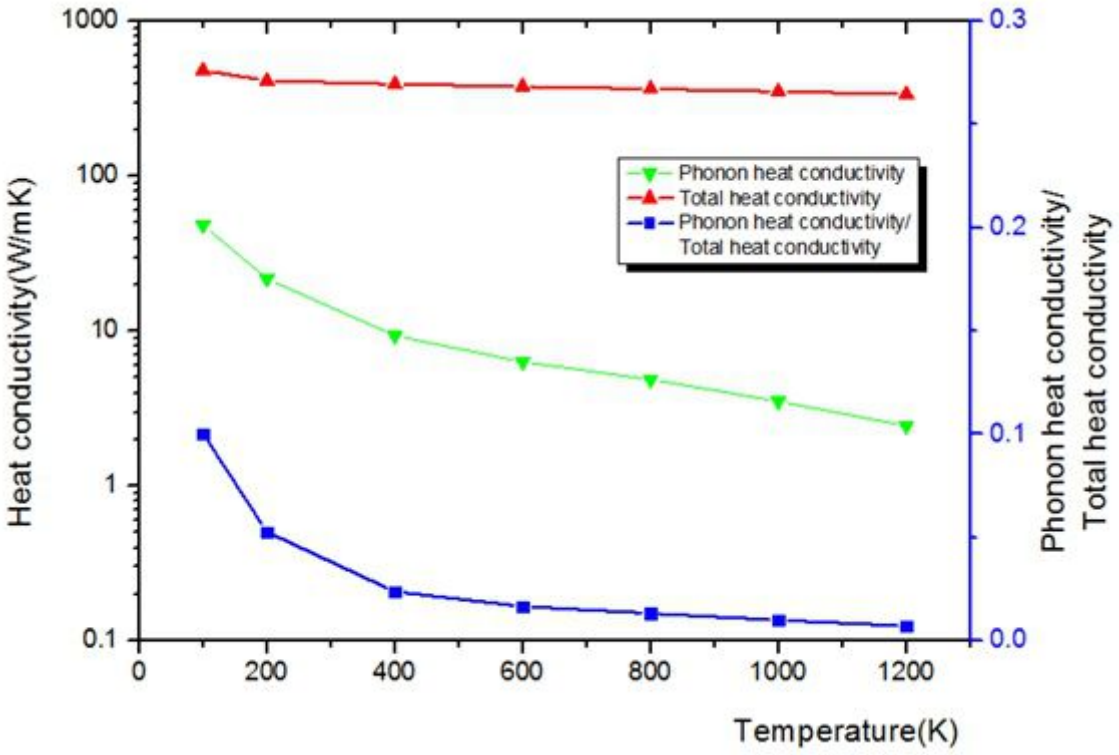

Figure 5- 4 The figure shows the total heat conductivity of copper (red line) in experiment, [41] the phonon heat conductivity (green line) obtained in molecular dynamics, and the ratio of the total heat conductivity to the phonon heat conductivity.

6 The effect of vacancy

This chapter explores the effect of vacancy on phonon heat conductivity (k) of Cu. Molecular dynamics method is put in use at different temperatures. Except the phonon heat conductivity, the HCACF of models with vacancy is investigated in details. The key of this work is to concern not the specific value of phonon heat conductivity of Cu with vacancy but the trend of k contaminated by vacancy. Note that the following models at different temperatures are not exactly the same.

6.1 Cu at 50 K

In this section we study the thermal property of pure Cu at 50 K. The goal is to study how its phonon heat conductivity changes with the increase of vacancy concentration.

6.1.1 Model

The model contains 4000 Cu atoms, at the start. The shape of the system is square, and it is definitely arranged as a Face Centred Cubic (FCC) lattice with the orientation x [1 0 0], y [0 1 0] and z [0 0 1]. The length of the system in x direction is 10σ as well as that in y and z direction. This model is almost identical to those used in Section 5.1. The crucial distinction is that some Cu atoms are taken away from the system resulting in the formation of vacancies. The geometrical configuration is displayed in Figure 6-1. Periodic boundary conditions are used along all three directions, x, y, z. The interactions of Cu atoms are modelled by the EAM potential proposed by Foiles.

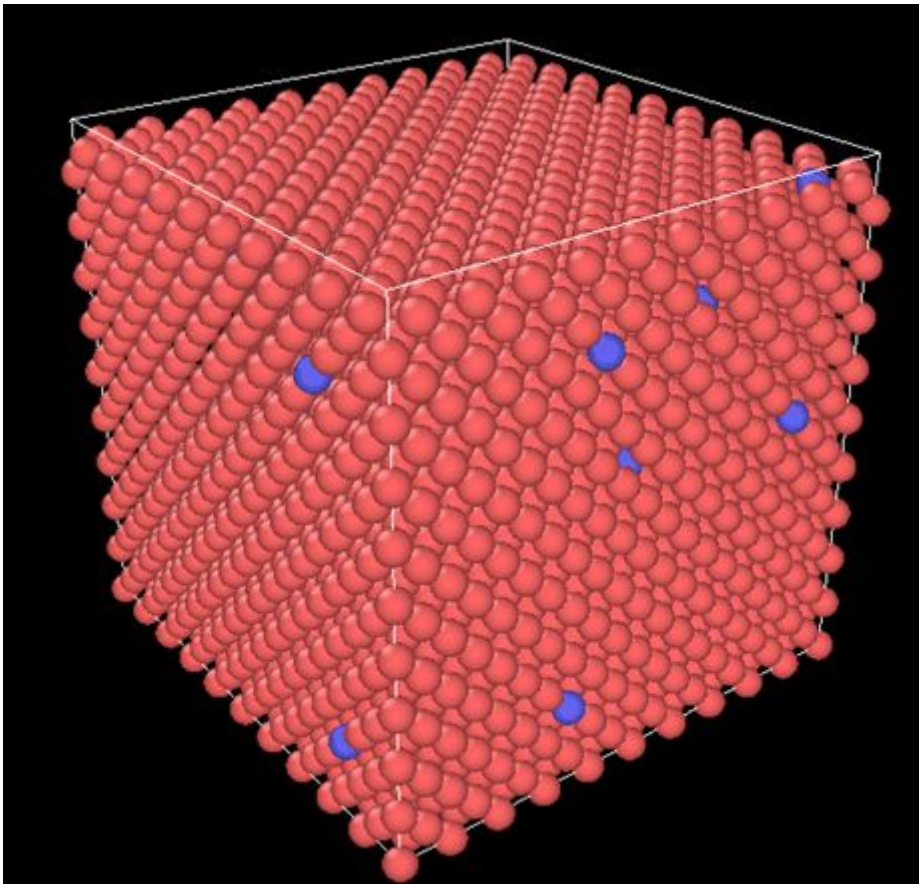

Figure 6-1 A schematic graph of a simulation model with vacancies. The red balls are Cu atom, while the blue one represent the vacancy position where the atom is removed.

Vacancies are induced by deleting atoms randomly in the model. In thesis, we define **vacancy concentration** (**vacancy fraction**) as the ratio of the number of atoms deleted to total atom number.

The time step of simulation is 0.01 ps. Firstly, the molecular dynamics simulation is implemented in a canonical ensemble (NVT) with simulation run time of 30 ps. After the temperature of the system is kept stable at 50 K, the simulation is performed for a further 10 ns running time in the micro-canonical ensemble (NVE). In the meantime, the phonon heat conductivity is obtained. Regarding the computation of HCACF, the correlation length is 100 ps, which provides HCACF adequate time to decay.

6.1.2 Results and Discussion

The phonon heat conductivity of copper has been obtained for different vacancy concentrations.

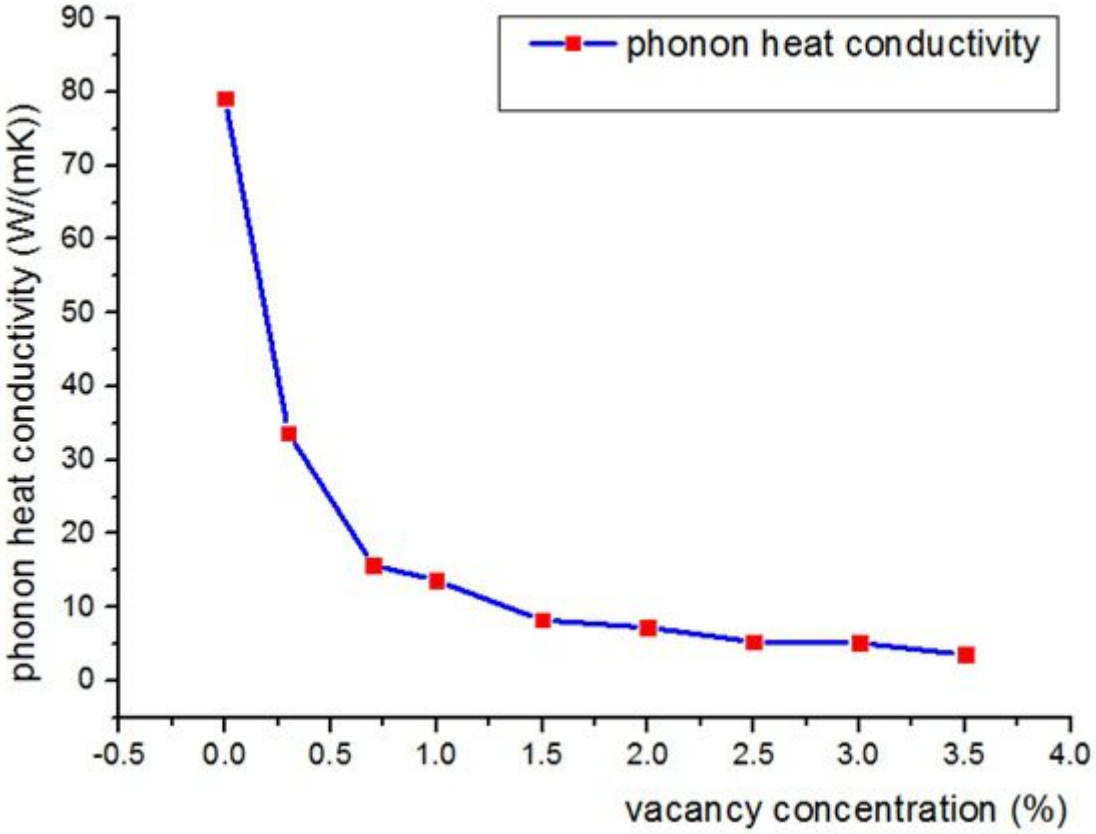

Figure 6-2 The phonon heat conductivity of pure copper as a function of vacancy concentration at 50 K.

Figure 6-2 shows the phonon heat conductivity of pure copper as a function of vacancy concentration at 50 K. As is indicated in Figure 6-2, the phonon heat conductivity of Cu decreases with the increasing vacancy concentration. Moreover, the drop can be separated into two stages. At the first stage, the phonon heat conductivity declines rapidly from about 80 W/(mK) in perfect system to approximately 16 W/(mK) with 0.7% of vacancy fraction. A linear relationship (see Figure 6-3) in this area can be obtained:

$$y=-8800x+72 \quad (6-1)$$

At the second stage where vacancy concentration begins from 0.7%, the graph shows a slow reduction and the phonon heat conductivity drops only by 12 W/(mK) from 0.7% to 3.5%. The relationship between phonon heat conductivity and vacancy concentration (see Figure 6-3) in this area can be expressed as,

$$y=-416x+16.9 \quad \textbf{(6-2)}$$

where x is the vacancy concentration and y is phonon heat conductivity.

The slope of the previous stage is 20 times of that of the following one. It means that the speed of the reduction in the first stage is greatly faster than that of the second. When the vacancy fraction becomes great enough, its effect on phonon heat conductivity is less sensitive than the circumstance of low fraction. This phenomena is discovered in other imperfect materials, such as graphene [26] and silicon [6].

The connection between phonon heat conductivity and vacancy concentration can be fitted in an exponential way,

$$y=72\exp(-300x)+6.25 \quad \textbf{(6-3)}$$

Compared to the linear fit, the exponential fit shows a better match and can explain in a more range of vacancy fraction.

The system has a total reduction of 95.5% in phonon heat conductivity with a 3.5% vacancy fraction.

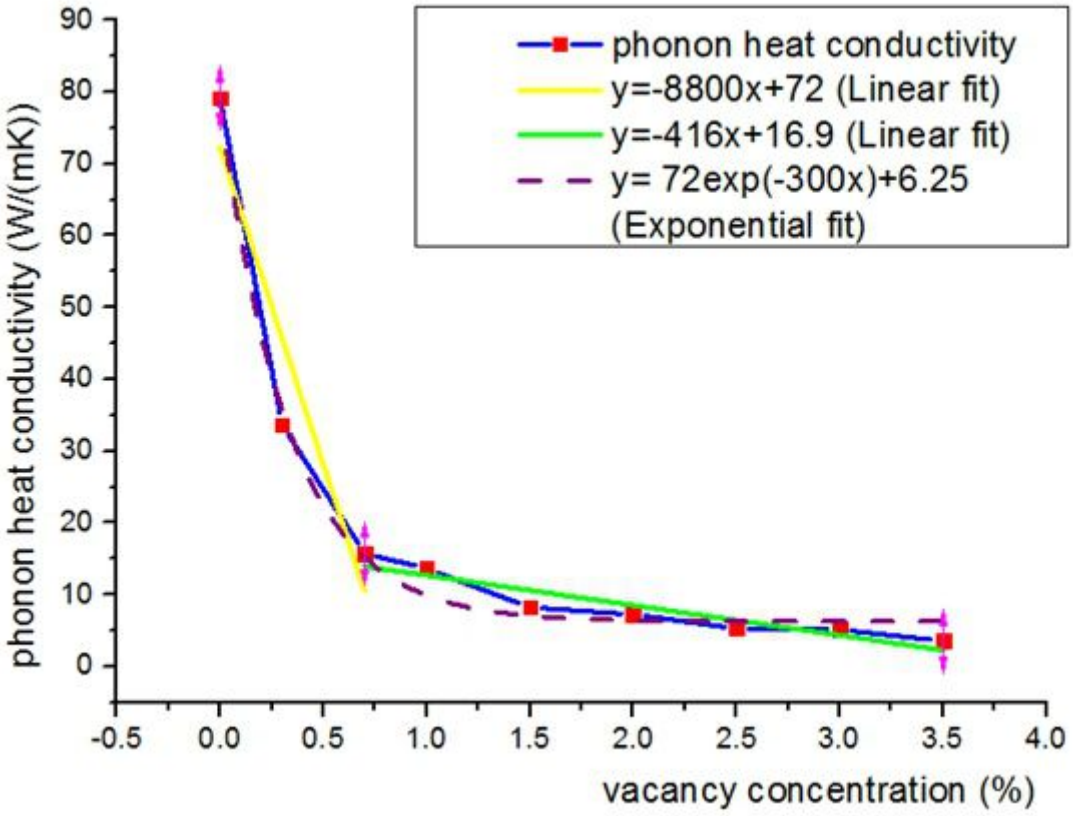

Figure 6-3 A picture of curve fitting between phonon heat conductivity and vacancy concentration in a Cu model at 50 K. The yellow and green solid line are linear fitting, while the purple dash one is exponential fitting.

The quality of HCACF is an important factor to the calculation of phonon heat conductivity. Figure 6-4 plots the normalized heat current autocorrelation function (HCACF) of pure copper with a 1% vacancy fraction at 50 K in the x, y, z direction. It can be seen from Figure 6-4 that the trajectories of HCACF are more or less the same in all three directions. In the following part, the HCACF in x direction is demonstrated as a representation. As indicated in Figure 6-4, the HCACF exhibits a complicated behaviour with time evolved. At first, the HCACF experiences a rapid drop to 0.32 at around 0.22 ps (see Figure 6-4, dot A) followed a relatively gentle grow. After it goes up to about 0.43 (see Figure 6-4, dot B), it begins to decrease more slowly until it finally converges at around 10 ps. On the whole, the HCACF of imperfect copper illustrates a similar behaviour as perfect copper at the same temperature, 50 K. (see Section 6.5.2)

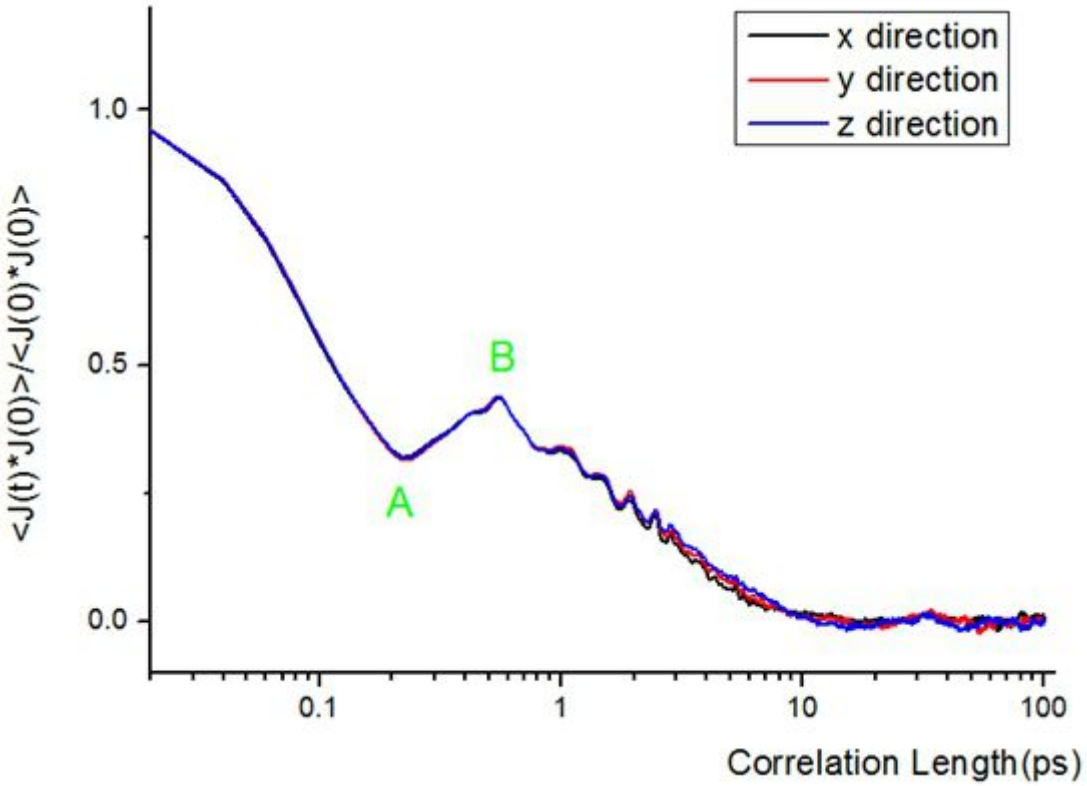

Figure 6-4 The normalized HCACF of pure copper with 1% vacancy fraction at 50 K in the x, y, z direction.

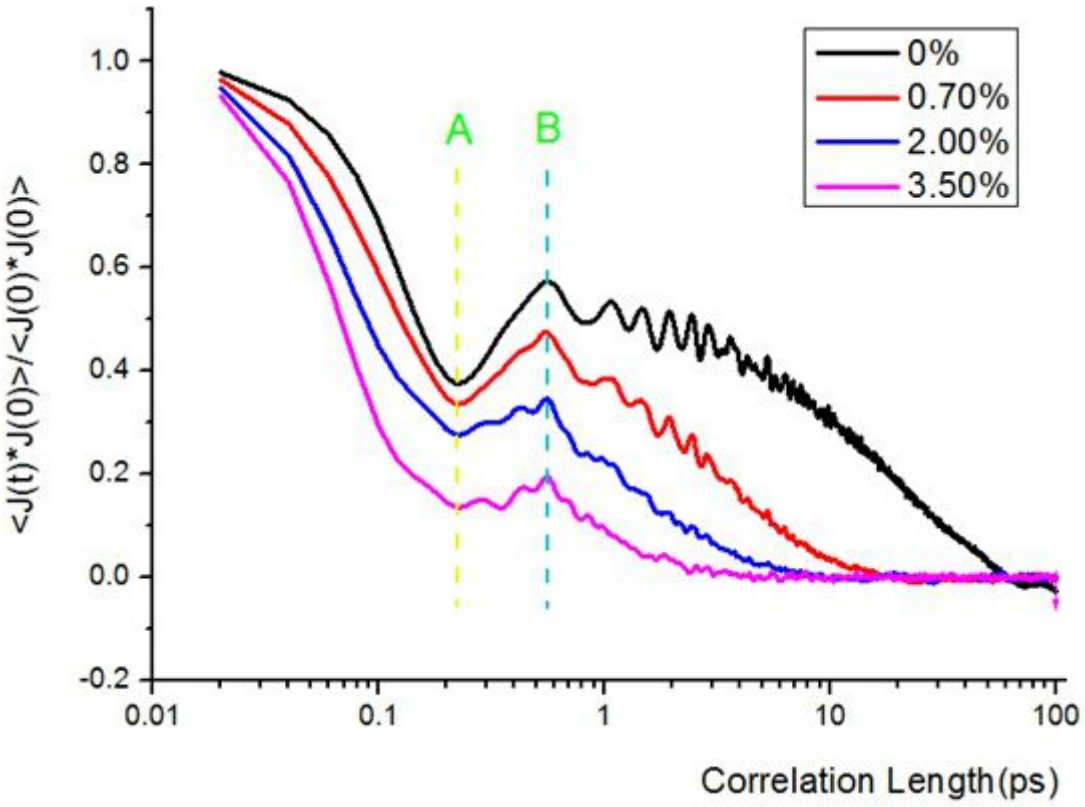

Figure 6-5 The normalized HCACF of pure copper with vacancy fraction 0%, 0.7%, 2.0% and 3.5% at 50 K. The result is the average value of the HCACF in x, y, z direction.

Figure 6-5 plots the normalized HCACF of Cu with vacancy fraction 0%, 0.7%, 2.0% and 3.5% at 50 K, which is the average value of the HCACF in all x, y, z direction. According to Figure 6-5, the HCACF shows a three-stage behaviour. First stage is a sharp decline, then followed by a rise, and the last one is a slight decay. The bottom of the first reduction is becoming lower and lower with the growth of vacancy fraction. At the same time, the peak of the second stage (the increase process following the rapid drop) falls as well with vacancy fraction.

With regard to the decay time of HCACF, it can be observed from the Figure 6-5 that the greater the vacancy concentration is, the more quickly the HCACF decays. The time of HCACF decay to zero in the 0.7% vacancy concentration model is about 17 ps, which is four times of that of 3.5% costs (4 ps). The most interesting finding is that not only the bottom of the first stage but also the peak

of the second stage appear at a specific time (0.22 ps and 0.56 ps, respectively) regardless of the vacancy fraction.

The first stage is associated with short wavelength, and the third stage is related with long wavelength. By introducing vacancy into the system, the length of phonon scattering becomes short resulting in the rapid decrease of HCACF. (Figure 6-5) With regards to the second stage, it rises due to the occurrence of a transverse wave. Likewise, the normalized HCACF decreases with vacancy concentration. Vacancy may also effect the scattering of transverse wave leading to the drop of HCACF.

6.2 Cu at 300 K

In this section we study the thermal property of pure copper at 300 K. The goal is to study how its phonon heat conductivity changes with the increase of vacancy concentration.

6.2.1 The Model

The model is based on previous one (section 6.1.1). The system is initially composed of 32000 copper atoms in a box with the dimensions of 20σ×20σ×20σ (σ=3.615) in x, y, z direction with the lattice structure FCC structure at 300K. Next step is to introduce vacancies by deleting atom randomly in the system. Periodic boundary conditions is applied in all three directions as well.

The time step of the system is 0.001 ps, and the correlation length of HCACF is 20 ps. The process of simulation is definitely separated into two parts, canonical (NVT) ensemble and microcanonical (NVE) ensemble, the simulation time of which is 2ns and 10ns, respectively.

6.2.2 Results and Discussion

The phonon heat conductivity of Cu with different vacancy concentrations at 300 K is shown in Figure 6-6. There is a clear downward trend of phonon heat conductivity with vacancy concentration.

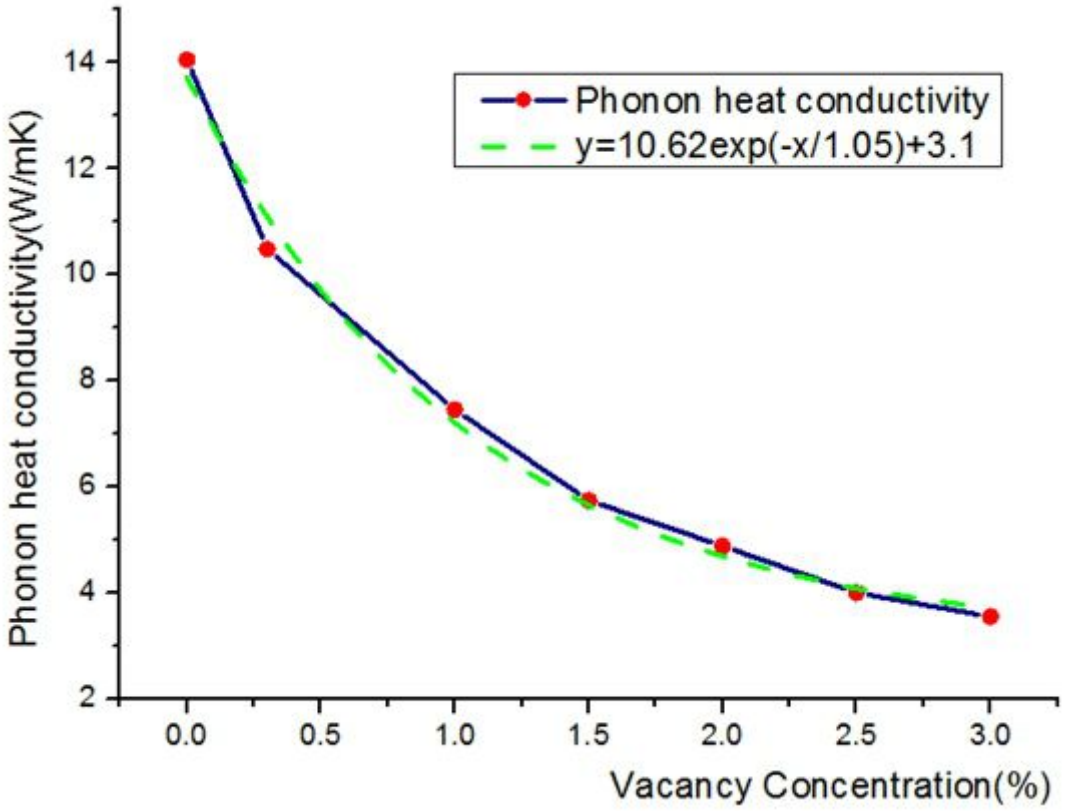

Figure 6-7 The phonon heat conductivity of pure copper as a function of vacancy concentration at 300 K.

The relationship between k and vacancy concentration can be fitted in an exponential way,

$$y=10.62\exp(-x/1.05)+3.1 \quad \textbf{(6-4)}$$

where x is the vacancy concentration and y is phonon heat conductivity.

As shown in Figure 6-6, equation 6-4 fits well.

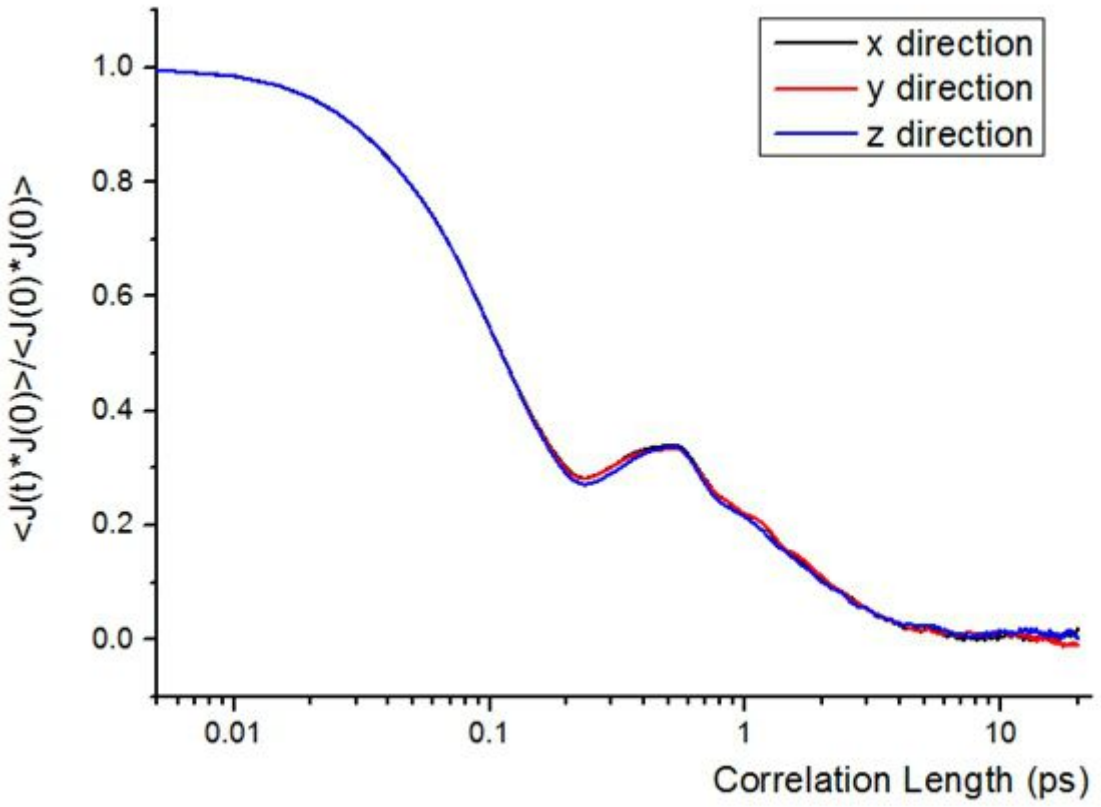

Figure 6-8 The normalized HCACF of pure copper with a 1% vacancy fraction at 300 K in the x, y, z direction.

Figure 6-7 shows the normalized HCACF of pure copper with 1% vacancy fraction at 300 K in the x, y and z direction. Each direction presents a similar trajectory. The normalized HCACF experiences a fast decline, then a slight increase and finally a much slower decay.

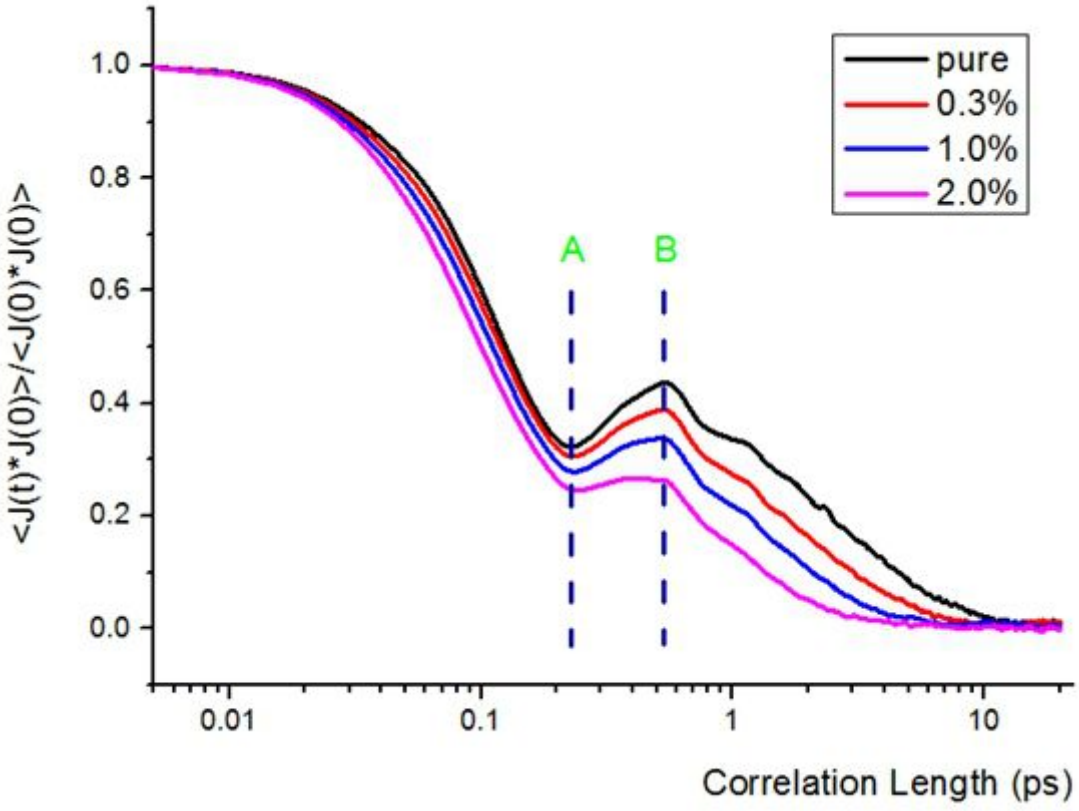

Figure 6-9 The normalized HCACF of pure copper with vacancy fraction 0%, 0.3%, 1.0% and 2.0% at 300 K. The result is the average value of the HCACF in x, y, z direction.

As illustrated in Figure 6-8, the greater the vacancy concentration is, the swifter the normalized HCACF decays. Vacancy impact the scattering of phonon, hence, the HCACF needs less time to decay to zero. Besides, Figure 6-8 shows the same phenomena happening in the model at 50 K. The dash line A and B present a bottom and a top, respectively. Besides, the time where A and B locate is much similar to that at 50 K, which are 0.23 ps and 0.54 ps, respectively.

6.3 Cu at 1000 K

In this section we study the thermal property of pure copper at 1000 K. The goal is to study how its phonon heat conductivity changes with the increase of vacancy concentration.

6.3.1 Model

To start with, the model is made up of 4000 copper atoms. The crystal structure is FCC with the length 10σ in all three axes. PBC is applied in all directions as well. The system produces vacancies by deleting atoms. Next step is to set the potential functions. The potential function of this model is the same as the previous ones.

After the structure and potential of the model is determined, it is implemented in NVT ensemble. However, the system starts to calculate phonon heat conductivity after 1 ns and the second stage simulation time is 10 ns. Besides, the correlation length of HCACF is 100 ps.

This model is similar to that in section 6.1.1. The difference between them is this simulation is implemented only in NVT ensemble. The reason is that this method can save a great deal of computational time due to the choice of high value time step. In my study, it is found that the time step is associated with the stability of temperature in NVE ensemble.

Figure 6-9 presents how time step effects temperature in NVE ensemble in a model of 300 K. (Section 5.2.1) The model is put into NVT ensemble and next NVE ensemble. As illustrated in Figure 6-9, the temperature (time step=0.01 ps) in NVE ensemble grows up hugely with running number of time steps, and there is a slightly upwards trend for that (time step=0.004 ps), only that (time step=0.001 ps) levels off. Therefore, it is appropriate to set the time step 0.001ps for keeping the system stable in that model. Nevertheless, the model (time step= 0.001 ps) costs much more time than the others in calculation in the condition of a certain simulation time. For instance, assuming that the

simulation time is 1ns, the model (time step=0.001 ps) is calculated in 1000 times, while that (time step=0.01 ps) only needs 100 times.

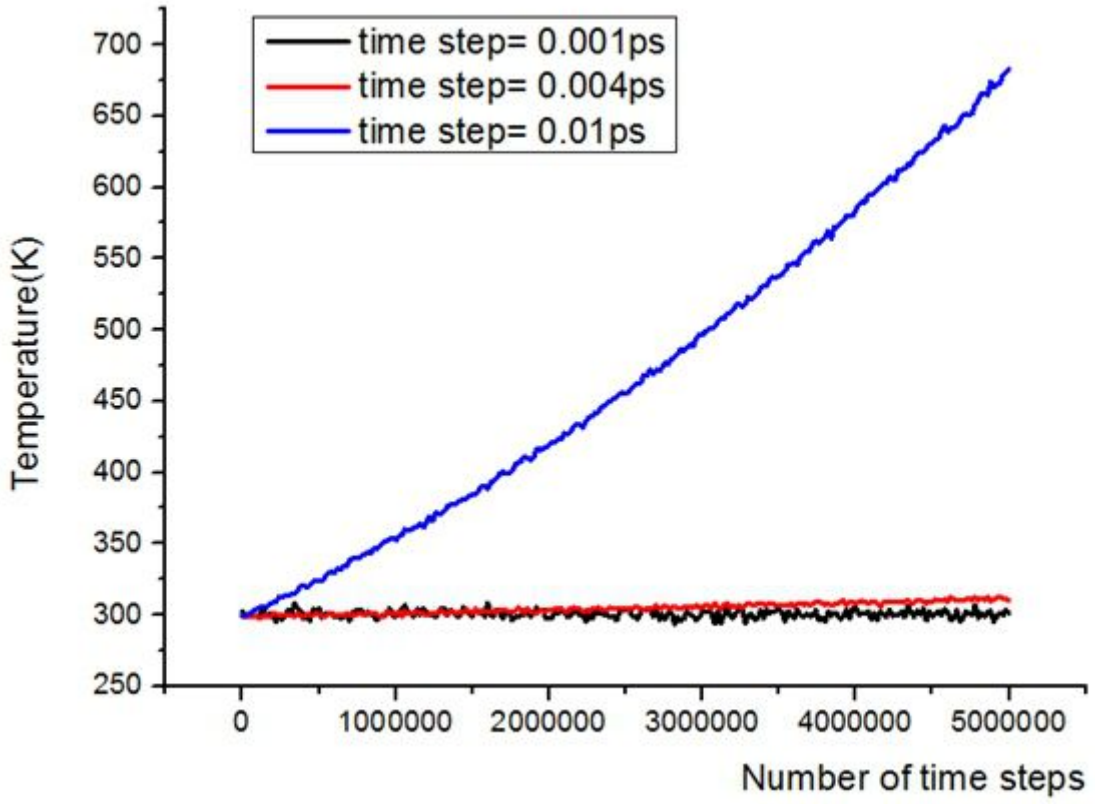

Figure 6-10 The temperature in NVE ensemble with time evolved. The initial temperature is 300 K.

However, we do not find the above phenomenon in the model that is only arranged in NVT ensemble. Thus, applying the method with a high time step can save enormous time.

6.3.2 Results and Discussion

Figure 6-10 plots the phonon heat conductivity of copper at 1000 K as a function of vacancy concentration. As indicated in Figure 6-10, the phonon heat conductivity decreases slowly with the increasing vacancy fraction. Nevertheless, distinct two stage behaviour occurring in the model at 50K and 300K does not happen.

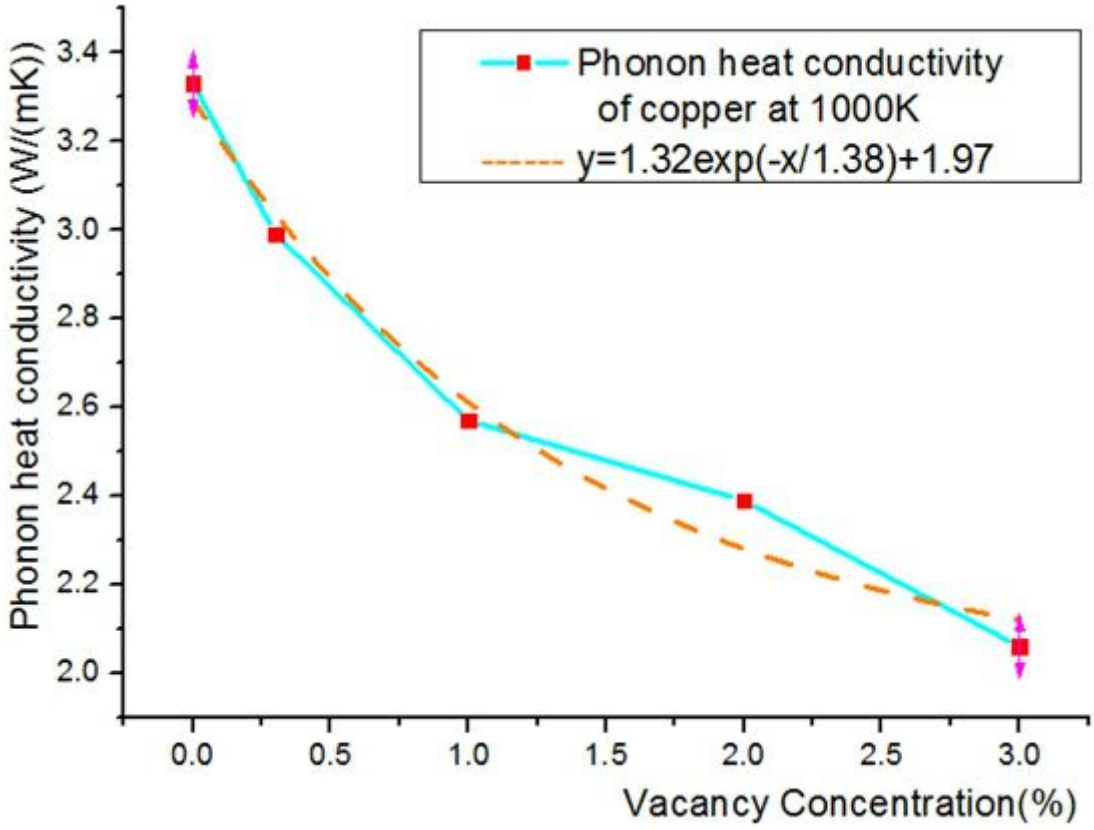

Figure 6-11 The phonon heat conductivity of pure copper as a function of vacancy concentration at 1000 K.

Related to how the vacancy effects the phonon heat conductivity, it can be defined by,

$$y=1.32\exp(-x/1.38)+1.97 \quad \textbf{(6-5)}$$

where x is the vacancy concentration and y is phonon heat conductivity.

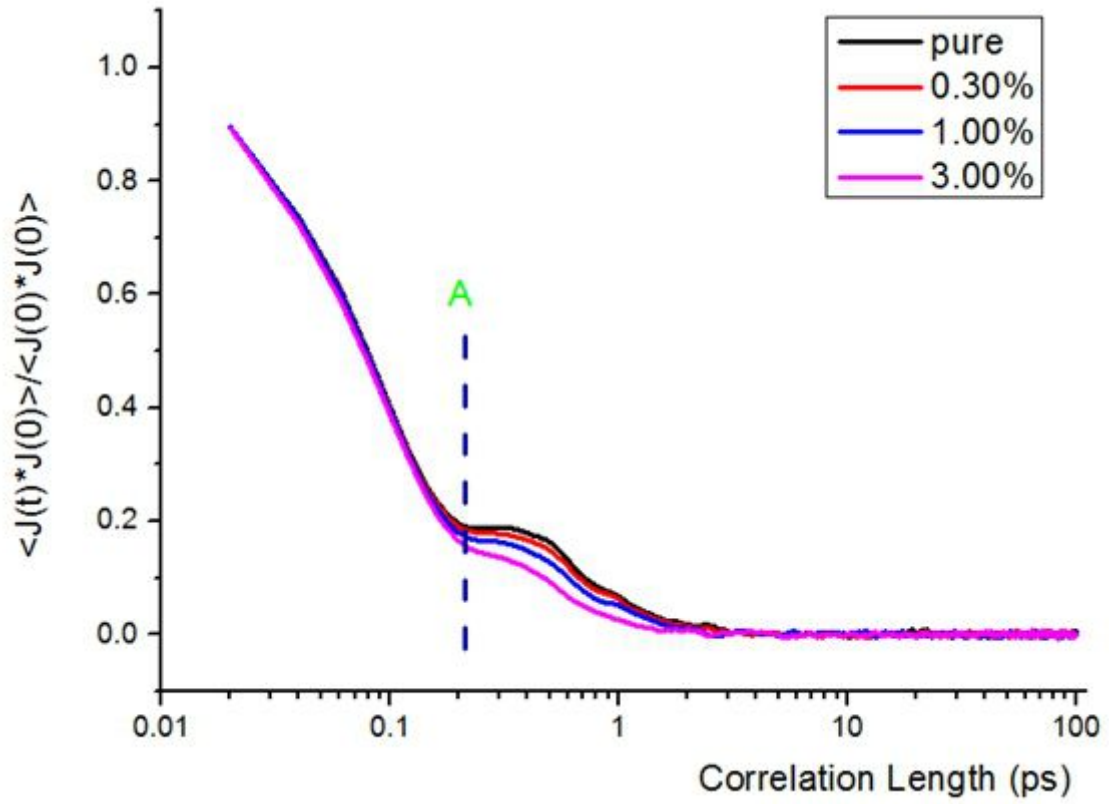

Figure 6-12 The normalized HCACF of pure copper with vacancy fraction 0%, 0.3%, 1.0% and 3.0% at 1000 K. The result is the average value of the HCACF in x, y, z direction.

Figure 6-11 shows the normalized HCACF of Cu with different vacancy concentrations at 1000 K. For the perfect copper, HCACF exhibits three stages, however, the second stage is not a clear growth but a shoulder, compared with the HCACF at 300 K. Moreover, the intersection point between the first and the second stage is nearly 0.22 ps (Plot A) similar to models at low and intermediate temperature. Regarding the shape of second stage, it presents not a rise but a shoulder due to decreasing effect of transverse wave. It can be explained in way that transverse wave affects worse in relatively low temperature than in relatively high temperature.

Concerning the imperfect model, it is hard to find a significant shoulder. Thus, the HCACF can be described into two decreasing stages. The first stage is faster than the second one.

The above explanation is referred to the shape of the HCACF. Relating to the value of the HCACF, it undoubtedly has a greater decay speed with a higher vacancy fraction because of vacancy. The HCACF of 3% vacancy concentration spends about 2.36 ps reaching the zero, whereas that of 0.3% vacancy concentration needs 3.58 ps.

6.4 Cu at 1300 K

In this section we study the thermal property of pure copper at 1300 K. The goal is to study how its phonon heat conductivity changes with the increase of vacancy concentration.

6.4.1 The Model

The model is similar to that at 1000 K. (Section 6.3.1) The only different parameter is temperature.

6.4.2 Results and Discussion

Figure 6-12 plots the phonon heat conductivity of copper at 1300 K as a function of vacancy concentration. It can be observed from Figure 6-12 that several results of imperfect copper are greater than that of perfect copper, which is totally different from the above low and intermediate temperature. Only when the vacancy concentration is 2% its phonon heat conductivity is lower than k_0 (phonon heat conductivity of perfect copper).

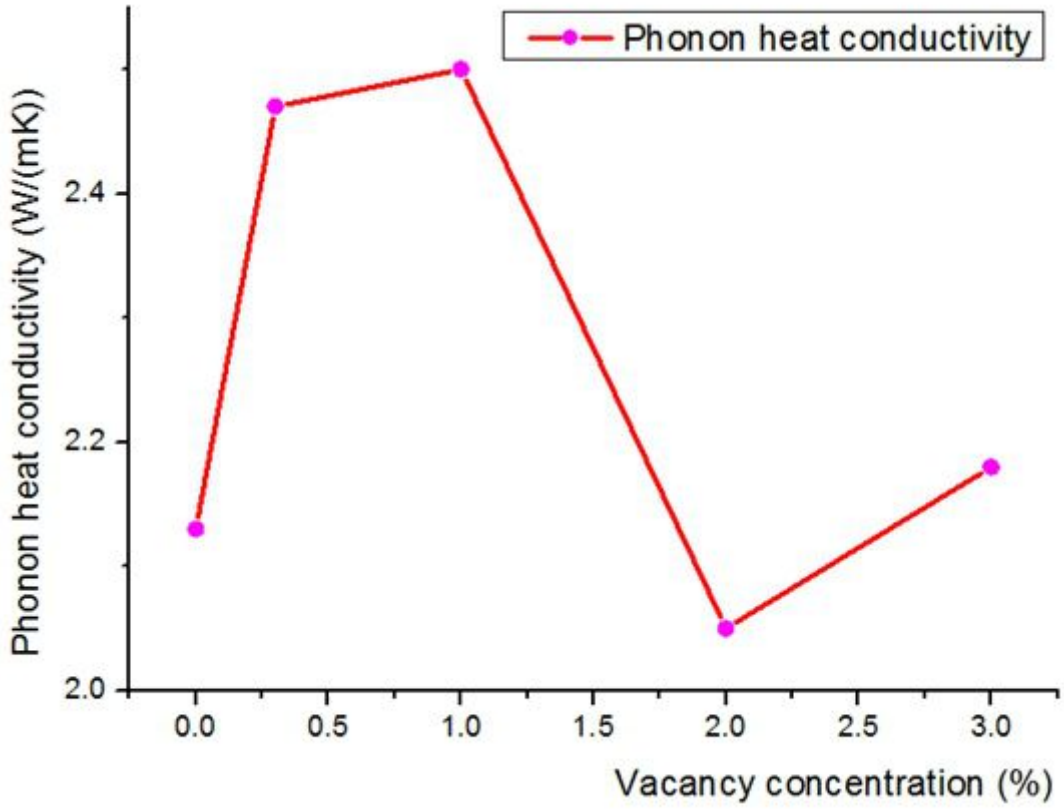

Figure 6-13 The phonon heat conductivity of pure copper as a function of vacancy concentration at 1300 K.

The Figure 6-13 displays the normalized HCACF of pure copper with vacancy concentration 0%, 0.3%, 1% and 2% at 1300 K. On one hand, as demonstrated in Figure 6-13, four normalized HCACF show a two-stage behaviour. At first, the curve drops rapidly, and then starts to decrease gently. The intermediate area between two stages locates at approximately 0.18-0.25 ps. On the other hand, it is still the truth that the HCACF in lower vacancy concentration decays faster than that in higher vacancy concentration.

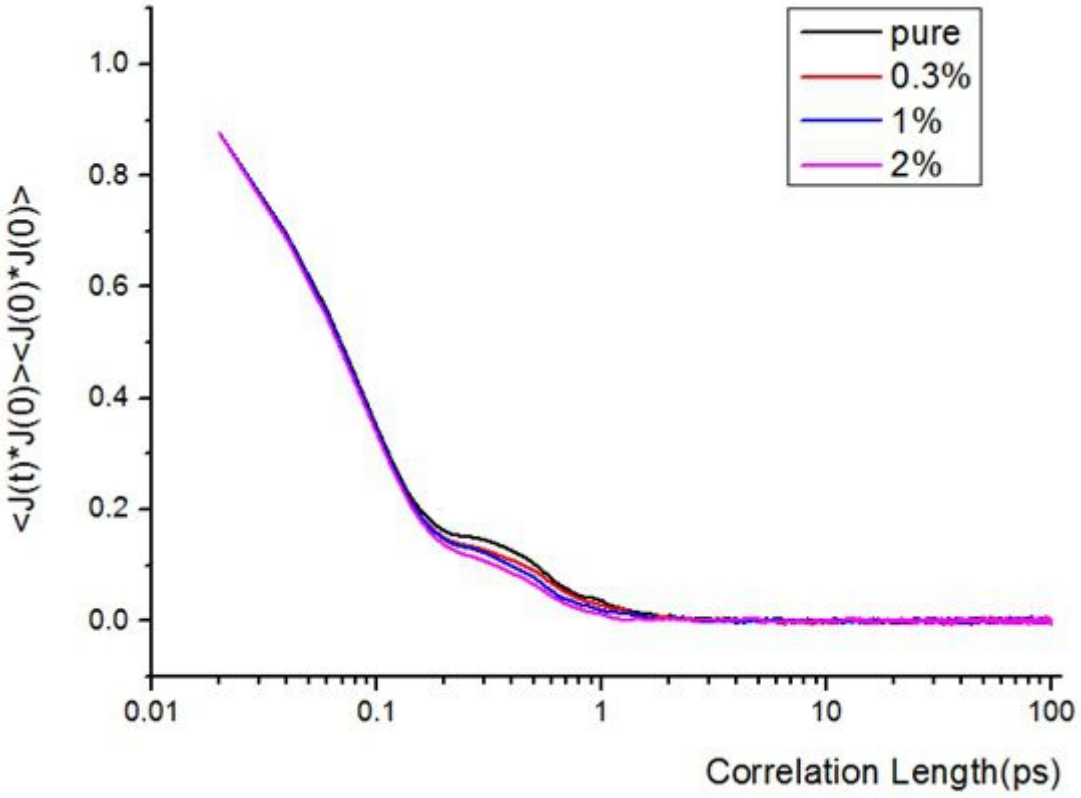

Figure 6-14 The normalized HCACF of pure copper with vacancy fraction 0%, 0.3%, 1.0% and 2.0% at 1300 K. The result is the average value of the HCACF in x, y, z direction.

It is undoubtedly that the normalized HCACF in low vacancy concentration is less than that in high vacancy concentration owing to vacancy similarly to the explanation in low and intermediate temperatures. (see Figure 6-13) According to above phenomenon, the phonon heat conductivity of perfect copper should be slightly greater than that of imperfect copper due to that phonon heat conductivity is the integral of HCACF. However, from Figure 6-12, there is no evidence presenting the phenomenon that the phonon heat conductivity decreases with vacancy fraction. The accumulated noise of the system may attribute to the occurrence of that abnormal circumstance. It is well-known that after HCACF decays to zero, it begins to fluctuate. At the same time, numerical noise is undoubtedly introduced in the computation of HCACF and results in the contamination of phonon heat conductivity. The calculation of HCACF can be

optimized by inducing a cut-off time. [64] Owing to the limited time of research, I did not try this new method.

6.5 Systematic Analysis and Discussion

This section explores the aggregate analysis of the above results. The aim is to explore the connection among different temperatures about how vacancies impact the phonon heat conductivity of Cu.

6.5.1 Value

As described previously, vacancy has a detrimental effect on phonon heat conductivity of Cu. In addition, the phonon heat conductivity decreases with the increasing vacancy concentration at all above temperatures excluding 1300K. The following explains the mechanism that vacancy effects phonon heat conductivity by the mean of kinetic theory.

According to the **kinetic theory**, the phonon heat conductivity can be approximated by,

$$k = \frac{1}{3} Cvl \qquad \textbf{(6-6)}$$

where C is the **specific heat capacity**, v is the **phonon group velocity of sound wave** in solid and ι is the **phonon mean free path**.

Leaving the electrons aside, the mean free path of copper is determined by the phonon-phonon scattering. Nevertheless, in this thesis, the mean free path is assumed as,

$$\frac{1}{l} = \frac{1}{l_{phonon-phonon}} + \frac{1}{l_{phonon-vacancy}} \qquad \textbf{(6-7)}$$

where $\iota_{\text{phonon-phonon}}$ is phonon-phonon scattering length and $\iota_{\text{phonon-vacancy}}$ is phonon-vacancy scattering length.

By equation 6-6 and equation 6-7, we can obtain,

$$\frac{1}{k} \propto \frac{1}{l_{phonon-phonon}} + \frac{1}{l_{phonon-vacancy}} \quad \textbf{(6-8)}$$

According to equation 6-8, 1/k is proportional to ($1/l_{phonon\text{-}phonon}+1/l_{phonon\text{-}vacancy}$). The phonon heat conductivity declines owing to the introduction of the scattering between phonon and vacancy. In other explanation way, the phonon mean free path l decreases due to phonon-vacancy scattering. Moreover, based on equation 6-6, the phonon heat conductivity drops resulting from the decrease of the phonon mean free path l. Hence, in case that C and v are constant, the phonon heat conductivity decreases with the increasing number of vacancies.

With respect to the kinetic theory, we can explain the affection on phonon heat conductivity in other ways. The mean free path can be defined by,

$$l = vt \quad \textbf{(6-9)}$$

where τ is relaxation time.

The mean free path l and the relaxation time τ stand for the average distance and time between two successive scattering events, respectively. The appearance of vacancy in Cu leads to the decrease of the relaxation time, hence, which gives rise to the reduction of the phonon heat conductivity of the system.

Figure 6-14 demonstrates the ratio of the phonon heat conductivity of imperfect copper (k) and that of perfect copper (k0) with different vacancy concentrations. From Figure 6-14, the ratio k/k0 decreases as the concentration grows up for all three temperatures. Moreover, the ratio with the same fraction rises with the reduction of temperature. For 1.0% vacancy fraction, k/k0 at 50 K is 17.2%, while that 1000 K is as many as 77.18%. It means that vacancy impacts the phonon heat conductivity of low temperature worse than that of high temperature.

As is expressed previously, the mean free path l decreases with temperature in metals. Therefore, it is reasonable that the effect of vacancy on high l associated with relatively low temperature is more sensitive than that of low l related to relatively high temperature.

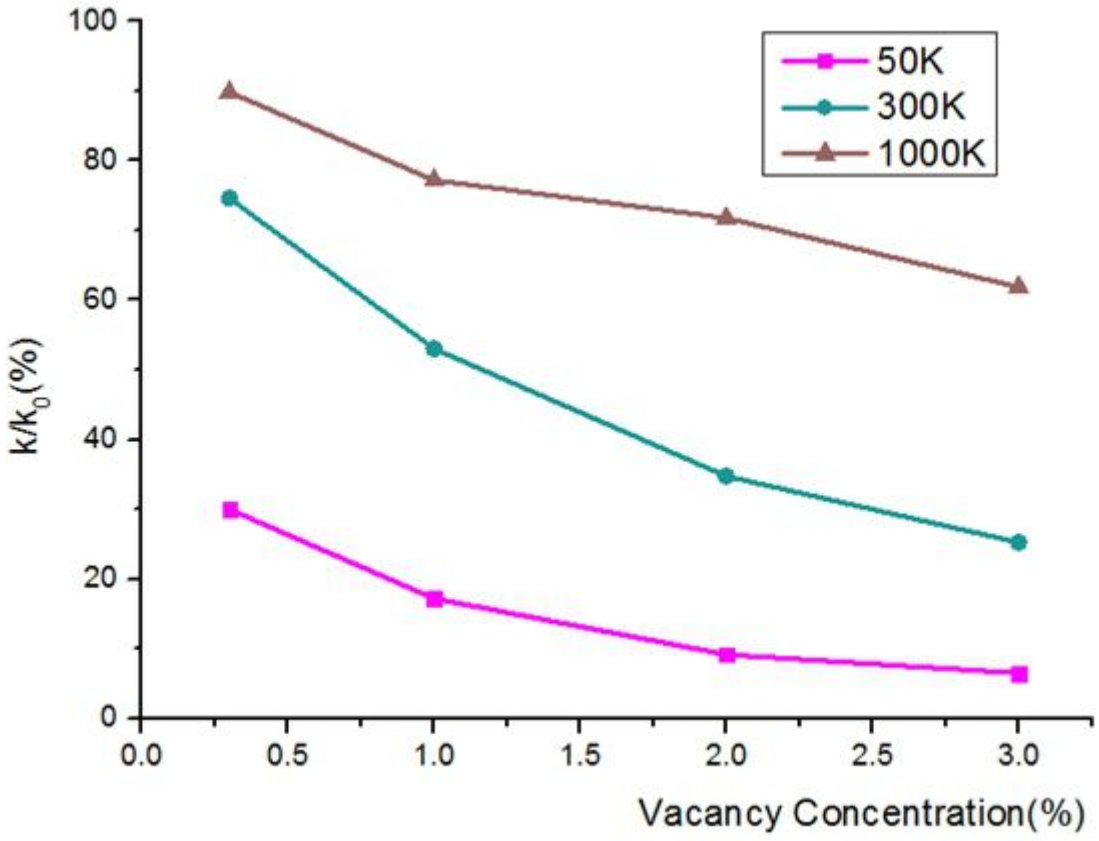

Figure 6-15 Normalized phonon heat conductivity k/k0 with vacancy concentration at 50 K, 300 K, 1000 K. k0 is the phonon heat conductivity of copper with 0% vacancy concentration.

6.5.2 HCACF

Here, we study that how vacancy impacts HCACF in different temperatures. First of all, we need to understand the behaviour of HCACF of perfect Cu. Figure 6-15 illustrates a schematic graph of the HCACF in 50 K, 300 K, 1000 K and 1300 K.

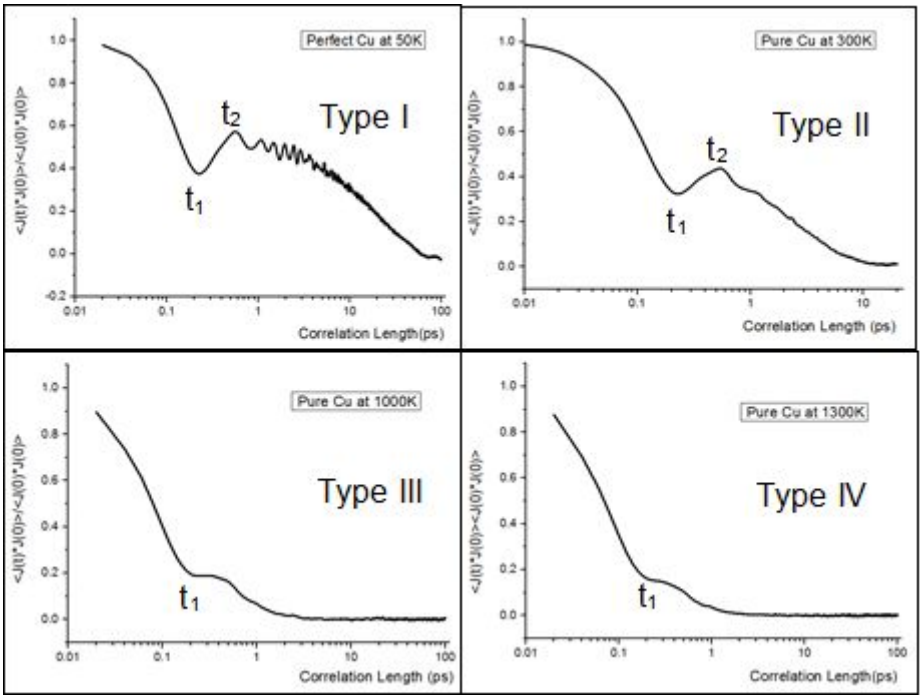

Figure 6- 16 A schematic graph of HCACF at 50K, 300K, 1000K and 1300K.

As shown in Figure 6-15, there are three stages for HCACF at 50 K, 300 K and 1000 K before it decays to zero. However, the HCACF of 1300 K only has two stages, a rapid decrease stage and a slow one. After the first rapid stage, the HCACF has a growth at 50 K and 300 K, besides, the level of the rise at 50 K is higher than 300 K. But for 1000 K, the second stage turns to a plateau. At last, HCACF declines slowly to zero and fluctuates at 50 K, 300 K and 1000 K. Note that the final decrease is full of oscillations at 50 K, and it becomes smooth with the increasing temperature.

The evolutionary process of HCACF with temperature can be described by Type I, Type II, Type III and Type IV (which presents HCACF shape of 50 K, 300 K, 1000 K and 1300 K, respectively) in order.

We define time of the bottom at first stage and the top at the second stage are t_1 and t_2, respectively in Type I and Type II. In Type III, t_1 is the intersection between the rapid decay and the plateau. In Type IV, t_1 is expressed as the intersection between two stages.

Next we discuss the effect of vacancy on HCACF.

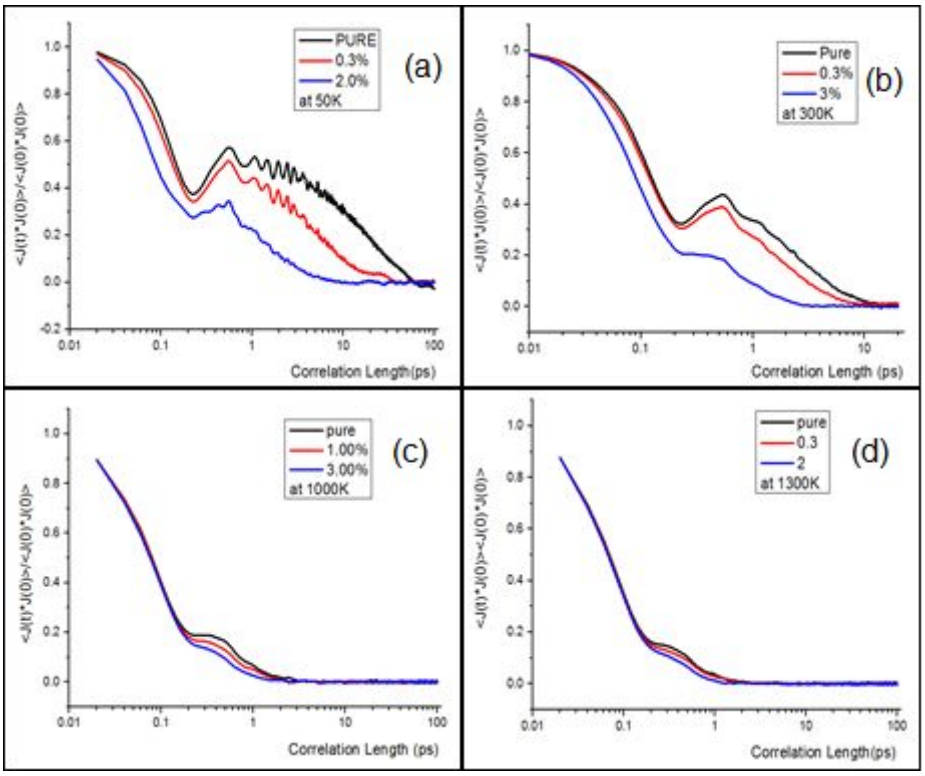

Figure 6-17 A schematic figure of the normalized HCACF with vacancy concentration. (a) 50 K, (b) 300 K, (c) 1000 K, (d) 1300 K.

The evolutionary manner of HCACF with vacancy concentration may be similar to that of temperature. It can be seen from Figure 6-16 (a) that the HCACF of the 50 K model with 2.0% vacancy fraction has a property of Type II, whereas that with 0.3% still has a shape of Type I. It means that there is a motivation of changing the shape of HCACF from Type I to Type II with the growth of vacancy fraction. The analogous phenomenon can be found at other temperatures. For instance, in Figure 6-16 (b), the HCACF of 3% belongs to not Type II but Type III at 300 K. Similarly, the shoulder disappears in the HCACF of 3% at 1000K (Figure 6-16 (c)). Only in the model of 1300 K (Figure 6-16 (d)), we cannot find the evolutionary process of HCACF due it has been the final pattern, Type IV.

All in all, the effect of vacancy on HCACF is similar to that of temperature, and the evolutionary sequence is Type I, Type II, Type III and Type IV as well.

With regards to the numerical value of HCACF, it absolutely decays faster with a higher vacancy fraction. This phenomenon can be observed in above all HCACF figures. Besides, both the HCACF of t_1 and that of t_2 of Type I and Type II with a relatively small vacancy fraction are greater than that with a relatively high one. Nevertheless, as mentioned earlier, they do not be altered with vacancy fraction. Especially, for t_1, it can be concluded that it is fixed at a specific amount or a small range for copper regardless of the temperature and vacancy fraction.

The rapid decay is associated with short wavelength phonons and the slow decay relates to long wavelength phonons. The above waves are longitudinal phonons, whereas the wave resulting in the second stage of Type I, II and III is transverse phonon.

6.6 Conclusions

In this chapter we have investigated how vacancy affects the phonon heat conductivity of Cu. The major findings can be summarized as follows:

- The phonon heat conductivity of copper decreases with the increase of vacancy concentration. Besides, we explain that the reduction of phonon heat conductivity is due to the scattering between phonon and vacancy by the kinetic theory
- The effect of vacancy on phonon heat conductivity at a lower temperature is more sensitive than that at a higher temperature
- The exponential fitting of the relationship between phonon heat conductivity and vacancy fraction exhibits better than the linear one
- Four types of HCACF are introduced. The point is that HCACF evolves in a specific sequence with the increasing vacancy similar to temperature

- We define the time when first rapid drop of HCACF ends as t_1. Moreover, it is concluded that t_1 is certain for Cu, regardless of either temperature or vacancy

7 Conclusions and Future Work

7.1 Conclusions

- A model of investigating the phonon heat conductivity of copper was built and validated. Moreover, it was improved to study the effect of vacancy on phonon heat conductivity.
- The phonon heat conductivity of copper decreases with the increase of vacancy concentration. Besides, we explain that the reduction of phonon heat conductivity is due to the scattering between phonon and vacancy by the kinetic theory
- The effect of vacancy on phonon heat conductivity at a lower temperature is more sensitive than that at a higher temperature
- The exponential fitting of the relationship between phonon heat conductivity and vacancy fraction exhibits better than the linear one
- Four types of HCACF are introduced. The point is that HCACF evolves in a specific sequence with the increasing vacancy similar to temperature
- We define the time when first rapid drop of HCACF ends as t_1. Moreover, it is concluded that t_1 is certain for copper, regardless of either temperature or vacancy

7.2 Future Work

- Although the computational model applied in this thesis is validated, it needs to be advanced, in many aspects of molecular dynamics techniques, such as, the simulation time and the Green-Kubo method.
- Until the present time, MD cannot describe the heat conductivity attributed by electrons. The most vital of future work is to improve the potential function.
- We have known some information about the effect of vacancy on phonon heat conductivity in molecular dynamics method. Hence, the next important step is experimental verification.
- The thesis has clarified the effect of vacancy on phonon heat conductivity. However, these findings needs an appropriate explanation in theory.
- Actually, vacancy is not the only defect in materials. It is a hard work to study other defects in molecular dynamics method.

REFERENCES

[1] Shabgard, H., Allen, M. J., Sharifi, N., Benn, S. P., Faghri, A., & Bergman, T. L. (2015). Heat pipe heat exchangers and heat sinks: Opportunities, challenges, applications, analysis, and state of the art. International Journal of Heat and Mass Transfer, 89, 138-158.

[2] von Böckh, P., & Wetzel, T. (2011). Heat transfer: basics and practice. Springer Science & Business Media.

[3] Nanohub.org,. (2008). nanoHUB.org - Resources: MSE 597G An Introduction to Molecular Dynamics. Retrieved 10 June 2015, from https://nanohub.org/resources/5838

[4] Schelling, P. K., Phillpot, S. R., & Keblinski, P. (2002). Comparison of atomic-level simulation methods for computing heat conductivity. Physical Review B, 65(14), 144306.

[5] Kaburaki, H., Li, J., Yip, S., & Kimizuka, H. (2007). Dynamical heat conductivity of argon crystal. Journal of Applied Physics, 102(4), 043514.

[6] Wang, T., Madsen, G. K. H., & Hartmaier, A. (2014). Atomistic study of the influence of lattice defects on the thermal conductivity of silicon. Modelling and Simulation in Materials Science and Engineering, 22(3), 035011.

[7] Plimpton, S., Crozier, P., & Thompson, A. (2007). LAMMPS-large-scale atomic/molecular massively parallel simulator. Sandia National Laboratories,18.

[8] Humphrey, W., Dalke, A., & Schulten, K. (1996). VMD: visual molecular dynamics. Journal of molecular graphics, 14(1), 33-38.

[9] A. Gittings, Cranfield University Astral HPC Cluster - User Guide - Issue 1.8. IT Department, Cranfield University, February 2014.

[10] Originlab.com., (2015). OriginLab - Origin and OriginPro - Data Analysis and Graphing Software. Retrieved 9 June 2015, from http://www.originlab.com/

[11] Reddy, G. P., & Gupta, N. (2010). Material selection for microelectronic heat sinks: An application of the Ashby approach. Materials & Design, 31(1), 113-117.

[12] Li, Q., Flamant, G., Yuan, X., Neveu, P., & Luo, L. (2011). Compact heat exchangers: A review and future applications for a new generation of high temperature solar receivers. Renewable and Sustainable Energy Reviews,15(9), 4855-4875.

[13] Tsai, C. Y., Chien, H. T., Ding, P. P., Chan, B., Luh, T. Y., & Chen, P. H. (2004). Effect of structural character of gold nanoparticles in nanofluid on heat pipe thermal performance. Materials Letters, 58(9), 1461-1465.

[14] Li, Y., Mei, D., Wang, H., Yao, Z., Zhu, T., & Chen, S. (2015). Reduced lattice thermal conductivity in nanograined Na-doped PbTe alloys by ball milling and semisolid powder processing. Materials Letters, 140, 103-106.

[15] Vincent, C., Silvain, J. F., Heintz, J. M., & Chandra, N. (2012). Effect of porosity on the thermal conductivity of copper processed by powder metallurgy. Journal of Physics and Chemistry of Solids, 73(3), 499-504.

[16] Kanatzidis, M. G. (2009). Nanostructured Thermoelectrics: The New Paradigm. Chemistry of Materials, 22(3), 648-659.

[17] Ying, T., Zheng, M. Y., Li, Z. T., & Qiao, X. G. (2014). Thermal conductivity of as-cast and as-extruded binary Mg – Al alloys. Journal of Alloys and Compounds, 608, 19-24.

[18] Ying, T., Zheng, M. Y., Li, Z. T., Qiao, X. G., & Xu, S. W. (2015). Thermal conductivity of as-cast and as-extruded binary Mg–Zn alloys. Journal of Alloys and Compounds, 621, 250-255.

[19] Carey, V. P., Chen, G., Grigoropoulos, C., Kaviany, M., & Majumdar, A. (2008). A review of heat transfer physics. Nanoscale and Microscale Thermophysical Engineering, 12(1), 1-60.

[20] Krupskii, I. N., & Manzhely, V. G. (1969). Multiphonon Interaction and the

heat Conductivity of Crystalline argon, Krypton, and Xenon. Soviet Physics JETP, 28(6), 1097-1100.

[21] Christen, D. K., & Pollack, G. L. (1975). Heat conductivity of solid argon. Physical Review B, 12(8), 3380.

[22] Kaburaki, H., Li, J., & Yip, S. (1998, January). Heat conductivity of solid argon by classical molecular dynamics. In MRS Proceedings (Vol. 538, p. 503). Cambridge University Press.

[23] Wang, X. W., Lee, H., Lan, Y. C., Zhu, G. H., Joshi, G., Wang, D. Z., ... & Ren, Z. F. (2008). Enhanced thermoelectric figure of merit in nanostructured n-type silicon germanium bulk alloy. Applied Physics Letters, 93(19), 193121.

[24] Yang, P., Li, X., Zhao, Y., Yang, H., & Wang, S. (2013). Effect of triangular vacancy defect on heat conductivity and heat rectification in graphene nanoribbons. Physics Letters A, 377(34), 2141-2146.

[25] Balandin, A. A., Ghosh, S., Bao, W., Calizo, I., Teweldebrhan, D., Miao, F., & Lau, C. N. (2008). Superior thermal conductivity of single-layer graphene. Nano letters, 8(3), 902-907.

[26] Hao, F., Fang, D., & Xu, Z. (2011). Mechanical and thermal transport properties of graphene with defects. Applied physics letters, 99(4), 041901.

[27] Wang, Y., Chen, S., & Ruan, X. (2012). Tunable heat rectification in graphene nanoribbons through defect engineering: A molecular dynamics study. Applied Physics Letters, 100(16), 163101.

[28] Yang, P., Li, X., Yang, H., Wang, X., Tang, Y., & Yuan, X. (2013). Numerical investigation on heat conductivity and heat rectification in graphene through nitrogen-doping engineering. Applied Physics A, 112(3), 759-765.

[29] Markussen, T., Jauho, A. P., & Brandbyge, M. (2009). Surface-Decorated Silicon Nanowires: A Route to High-Z T Thermoelectrics. Physical review letters, 103(5), 055502.

[30] Markussen, T., Jauho, A. P., & Brandbyge, M. (2009). Electron and phonon transport in silicon nanowires: Atomistic approach to thermoelectric properties. Physical Review B, 79(3), 035415.

[31] Lee, Y., Lee, S., & Hwang, G. S. (2011). Effects of vacancy defects on thermal conductivity in crystalline silicon: A non-equilibrium molecular dynamics study. Physical Review B, 83(12), 125202.

[32] Chantrenne, Raynaud, & Barrat. (2003). Study of phonon heat transfer in metallic solids from molecular dynamic simulations. Microscale Thermophysical Engineering, 7(2), 117-136.

[33] Yuan, S. P., & Jiang, P. X. (2006). Thermal conductivity of small nickel particles. International journal of thermophysics, 27(2), 581-595.

[34] Heino, P., & Ristolainen, E. (2003). Heat conduction at the nanoscale in some metals by MD. Microelectronics journal, 34(9), 773-777.

[35] Evteev, A. V., Momenzadeh, L., Levchenko, E. V., Belova, I. V., & Murch, G. E. (2014). Molecular dynamics prediction of phonon-mediated heat conductivity of fcc Cu. Philosophical Magazine, 94(7), 731-751.

[36] Feng, B., Li, Z., & Zhang, X. (2009). Role of phonon in the thermal and electrical transports in metallic nanofilms. Journal of Applied Physics,105 (10), 104315.

[37] Zumdahl, S. S., & Zumdahl Susan, A. (2007). Chemistry Seventh Edition.

[38] Mitchell B. S. (2004). An introduction to materials engineering and science, John Wiley & Sons, Inc,

[39] Callister, W. D. and Rethwisch, D. G. (2013), Materials science and engineering: an introduction, 9th ed, John Wiley & Sons, Inc, New York.

[40] Hull, D., & Bacon, D. J. (2011). Introduction to dislocations, 5th ed, Elsevier.

[41] Incropera, F. P. (2011). Fundamentals of heat and mass transfer, 7th ed, John Wiley & Sons.

[42] Lienhard, J. H. (2013). A heat transfer textbook. Courier Corporation.

[43] S. Middleman, An Introduction to Mass and Heat Transfer, Wiley: New York, 1998

[44] Holman, J. P. Heat Transfer. McGraw-Hill

[45] Rohsenow, W. M. (1998). Handbook of heat transfer (Vol. 3). New York: McGraw-Hill.

[46] Lejcek, P. (2010). Grain boundary segregation in metals (Vol. 136). Springer Science & Business Media.

[47] Jorgensen, W. L., & Tirado-Rives, J. (1996). Monte Carlo vs molecular dynamics for conformational sampling. The Journal of Physical Chemistry,100 (34), 14508-14513.

[48] Andrew R. Leach. (2001). Molecular modelling: principles and applications. Pearson Education.

[49] Jones J E. On the determination of molecular fields. II. From the equation of state of a gas [J]. Proceedings of the Royal Society of London. Series A, Containing Papers of a Mathematical and Physical Character, 1924: 463-477.

[50] Daw M S, Baskes M I. Embedded-atom method: Derivation and application to impurities, surfaces, and other defects in metals [J]. Physical Review B, 1984, 29(12): 6443.

[51] Daw, M. S., Foiles, S. M., & Baskes, M. I. (1993). The embedded-atom method: a review of theory and applications. Materials Science Reports, 9(7), 251-310.

[52] S. M. Foiles, M. I. Baskes, and M. S. Daw, “Embedded-atom-method functions for the fcc metals Cu, Ag, Au, Ni, Pd, Pt and their alloys”, Phys. Rev. B Vol.33, No.12, 1986

[53] Zalizniak, V. E. INTERATOMIC INTERACTION IN FCC METALS.

[54] Baskes, M. I. (1992). Modified embedded-atom potentials for cubic materials and impurities. Physical Review B, 46(5), 2727.

[55] Maruyama, S. (2000). Molecular dynamics method for microscale heat transfer. Advances in numerical heat transfer, 2(6), 189-226.

[56] Rapaport, D. C. (2004). The art of molecular dynamics simulation. Cambridge university press.

[57] Verlet, L. (1967). Computer" experiments" on classical fluids. I. Thermodynamical properties of Lennard-Jones molecules. Physical review,159(1), 98.

[58] Allen, M. P. (2004). Introduction to molecular dynamics simulation. Computational Soft Matter: From Synthetic Polymers to Proteins, 23, 1-28.

[59] Jabbarzadeh, A., & Tanner, R. I. (2006). Molecular dynamics simulation and its application to nano-rheology. Rheology Reviews, 2006, 165.

[60] Evteev, A. V., Momenzadeh, L., Levchenko, E. V., Belova, I. V., & Murch, G. E. (2015). Vibrational contribution to heat transport in liquid cooper: Equilibrium molecular dynamics study. Computational Materials Science, 96, 229-236.

[61] McGaughey, A. J. H., & Kaviany, M. (2004). Thermal conductivity decomposition and analysis using molecular dynamics simulations. Part I. Lennard-Jones argon. International Journal of Heat and Mass Transfer,47(8), 1783-1798.

[62] McGaughey, A. J., & Kaviany, M. (2006). Phonon transport in molecular dynamics simulations: Formulation and heat conductivity prediction. Advances in Heat Transfer, 39, 169-255.

[63] Kubo, R. (1957). Statistical-mechanical theory of irreversible processes. I. General theory and simple applications to magnetic and conduction problems. Journal of the Physical Society of Japan, 12(6), 570-586.

Kubo, R., Yokota, M., & Nakajima, S. (1957). Statistical-mechanical theory of irreversible processes. II. Response to thermal disturbance. Journal of the Physical Society of Japan, 12(11), 1203-1211.

[64] Chen, J., Zhang, G., & Li, B. (2010). How to improve the accuracy of equilibrium molecular dynamics for computation of thermal conductivity. Physics Letters A, 374(23), 2392-2396.

[65] Stackhouse, S., & Stixrude, L. (2010). Theoretical methods for calculating the lattice thermal conductivity of minerals. Reviews in Mineralogy and Geochemistry, 71(1), 253-269.

[66] Che, J., Çağın, T., Deng, W., & Goddard III, W. A. (2000). Thermal conductivity of diamond and related materials from molecular dynamics simulations. The Journal of Chemical Physics, 113(16), 6888-6900.

[67] Michael Frank. (2015). Molecular Studies of Confined Liquids and Nanofluids for Passive Thermal Management. Cranfield University

APPENDICES

Appendix A Units

A.1 Metal Units

The model of this work uses the Metal Units of LAMMPS. The followings are corresponding relationship between physical variables and units.

Table A. 1 Chart of unit of physical variable.

Physical Variable	Units
Time	Picosecond (ps)
Mass	Grams/mole (g/mol)
Distance	Angstroms (Å)
Energy	Electron volt (eV)
Velocity	Angstroms/picosecond (Å/ps)
Temperature	Kelvin (K)

A.2 Time Units

This section describes the conversion table of time units.

Table A. 2 Conversion Table of Time Units

Time Unit	Corresponding Magnitude
Millisecond (ms)	10^{-3} s
Microsecond (μs)	10^{-6} s
Nanosecond (ns)	10^{-9} s
Picosecond (ps)	10^{-12} s